

# Disaster Risk Analysis of a Power Grid Network

A thesis submitted to the Delft University of Technology in partial fulfillment  
of the requirements for the degree of

Master of Science in Engineering and Policy Analysis

by

Jin Rui Yap

Student number: 5039983

May 2021

First supervisor:	J. H. Kwakkel,	Policy Analysis, TU Delft
Second supervisor:	M. E. Warnier,	Systems Engineering, TU Delft
External supervisor:	O. A. Ishizawa,	World Bank Group
External supervisor:	J. M. Díaz,	World Bank Group

## Acknowledgements

There are many words that encapsulate the experience of completing this project: dizzying is one of those words, satisfying is another. The project thus far has *been* a learning experience, and I have very many people to thank for it. But, to name a few...

To my advisors who have patiently shared their time with me in order to walk me through the nitty-gritty bits of the project, thank you. It is highly unlikely that this project would have been submitted at the time of writing without your guidance over the past months.

And then, of course, the EPA and TU Delft community that has helped me through this project (and, really, the past two years) in so many ways. Notably, thank you Aarthi and Ignasi for your excellent proofreading, thank you Sangitha for patiently teaching me load flow analyses, thank you Trivik for taking the time to walk through my model-related confusions, and thank you Sahiti and Mikhail for gracefully taking on the role of go-to person for basically any and all questions.

Lastly, thank you to all family and friends who have been around even as I sank myself into the depths of this project. Most of all, to my parents, who may not always understand the why's and what's of what I want to do, but who nonetheless give me everything so that I can do it.

## Executive Summary

Cascading failures in power generation and transmission networks are an increasingly common and pressing issue given growing infrastructure interconnectivity. Meanwhile, climate-related hazards (such as floods) occur with mounting frequency and intensity, triggering initial failures that can cause a cascade through the network. It is in the interest of policy makers to invest in infrastructure upgrades and disaster risk management measures to reduce the frequency and magnitude of such failures. In many countries where sophisticated data collection and management systems are in place, such policies can be backed with data-driven analysis catered to country-specific contexts and needs. Unfortunately, the unavailability of such relevant data in other, often low-income, countries precludes this possibility. However, with the increasing sophistication of data collection technologies and data analysis techniques, more and more global data sets can be produced by combining high-resolution data sources with advanced data processing algorithms. The proliferation of such high-resolution global data sets creates the possibility of implementing data-driven analyses to support policy-making in environments where it has not been historically feasible.

In this research, we introduce a method for using global data sets to conduct a flood risk and cascading failures analysis in countries where high-quality data does not exist. As the goal is to support policy-making on a national level, an impacts analysis is additionally proposed to provide a systematic way of comparing system performance against multiple objectives and under potential policy interventions. The method proposed in this study provides policy makers with an avenue to conduct such an analysis in countries where the requisite data may not exist or is unavailable, thus paving the way for a data-driven approach to decision-making.

The global data sets used in this study consist of information about a country's river basins and flood risk, power system properties, and socio-economic indicators. A global data set providing river basin and flood risk information is first used to generate a high-resolution (90m) cell grid over the country, with each cell indicating the flood height at that location for a given flood scenario. These maps are overlaid with power network topology, derived from a separate global data set, to identify power system components that are exposed to flood risk. The level of risk faced by each component is then estimated using fragility curves.

Cascading failures are subsequently simulated in a model where initial failures are represented by the power network components identified in the flood risk analysis. Once the cascading failures are simulated, the geographic extents of the power outages can be plotted and identified. We showcase a method for using open survey data, which is available for over 90 countries, to estimate local population statistics in those areas. Based on this estimation, the impacts of the cascading failures can then be quantified not just in terms of total loss in power demand but also in terms of characteristics of the populations impacted. Within the case study, the number of poor households and the number of women-headed households impacted were analysed. To demonstrate one example, we apply the proposed method to the case study country of Sierra Leone.

This report further shows that the above analyses can be further built upon to analyse the impact of potential policy interventions and uncertain future scenarios. Based on the context of the case study location, we show ways in which this method can be used to assist the

consideration of policy interventions and to understand the potential impacts of climate change. The method may be used to analyse other types of policies and scenarios. Furthermore, the method can also be flexibly adapted to analyse other metrics for impacts assessment (e.g., levels of industrial activity in areas impacted) and other hazards (e.g., tropical storms), pending data availability.

Within the case study context, we demonstrate how the global data sets can be supplemented with country-specific information for increased accuracy of model inputs. We used country data from verified sources to validate the proposed method, specifically the components of power network generation and socioeconomic characteristics of the population. Some discrepancies were found and the methods to account for it have been discussed as part of future work. Having said that, the proposed method provides a promising approach for circumventing data availability constraints and equips policymakers with the ability to conduct a timely and approximate disaster risk analysis of a power network where it was not previously feasible.

## Contents

<b>1</b>	<b>Introduction</b>	<b>1</b>
1.1	Research objectives and questions . . . . .	2
1.2	Research approach . . . . .	4
1.3	Thesis outline . . . . .	4
<b>2</b>	<b>Literature Review</b>	<b>6</b>
2.1	Modelling of power networks . . . . .	6
2.2	Simulation and impacts of climate-related hazards . . . . .	8
2.3	Impact assessments . . . . .	9
<b>3</b>	<b>Method Implementation</b>	<b>11</b>
3.1	Power network representation . . . . .	11
3.1.1	MATCASC model and requirements . . . . .	11
3.1.2	Power network processing . . . . .	13
3.1.3	Power supply and consumption . . . . .	14
3.1.4	Transmission line properties . . . . .	15
3.2	Flood risk analysis . . . . .	15
3.3	Impacts quantification . . . . .	19
3.4	Other considerations . . . . .	20
3.4.1	Policy evaluation . . . . .	20
3.4.2	Climate change impacts . . . . .	20
<b>4</b>	<b>Case Study Application</b>	<b>22</b>
4.1	Country overview . . . . .	22
4.2	Sierra Leone power network . . . . .	23
4.3	Flood risk in Sierra Leone . . . . .	26
4.4	Quantifying impacts . . . . .	27
4.5	Policy evaluation . . . . .	28

---

4.6	Climate change impacts . . . . .	29
4.7	Validation and sensitivity analysis . . . . .	30
<b>5</b>	<b>Results</b>	<b>32</b>
5.1	Flood risk analysis . . . . .	32
5.2	Cascading failures analysis . . . . .	34
5.3	Policy Considerations . . . . .	35
5.4	Climate change impacts . . . . .	37
5.5	Validation and sensitivity analysis . . . . .	40
<b>6</b>	<b>Discussion</b>	<b>44</b>
6.1	Findings . . . . .	44
6.2	Validation and sensitivity analysis . . . . .	45
<b>7</b>	<b>Conclusion</b>	<b>48</b>
7.1	Research questions . . . . .	48
7.2	Impact of research . . . . .	50
7.3	Limitations . . . . .	51
7.4	Future directions of research . . . . .	52
<b>A</b>	<b>Appendix</b>	<b>58</b>
A.1	Policy Options . . . . .	59
A.2	Cascading failures in each damage state scenario . . . . .	60
A.3	Validation . . . . .	63
A.4	Sensitivity Analysis . . . . .	65

## List of Figures

1	Summary of data sources, data processing activities and analysis process. . . . .	11
2	Summary of inputs and outputs of MATCASC as adapted for this research . . . .	12
3	Demonstration of input and output of network simplification process. . . . .	14
4	Clustering of hexagon cells into clusters. . . . .	15
5	Example of a curve relating exceedance probability to hazard intensity. . . . .	16
6	Process for identifying a grid cell flood height for a given a river basin flood event.	17
7	View of network node with a 100m-diameter buffer, representing the Kingtom generation station in Freetown, Sierra Leone. . . . .	18
8	Fragility curves approximated from depth-damage values for electric system com- ponents. . . . .	18
9	Lines directly connected to a failed node are indicated as initial line threats. . . .	19
10	Projected change in average maximum 1-day precipitation. . . . .	21
11	Overview of simplified GridFinder data for Sierra Leone. . . . .	23
12	Overview of the GridFinder network cleaning process. . . . .	24
13	Process of generating, filtering, and clustering hexagon cells. . . . .	24
14	Processed network data for Sierra Leone. . . . .	25
15	Visual representation of one flood scenario. . . . .	26
16	Maps indicating proportion of vulnerable households, based on interpolated statis- tics. . . . .	27
17	Graphical representation of 3 of 120 iterations of link additions to the network. .	28
18	Flood maps for one example scenario, modified to account for projected climate change impacts. Inset maps show projected change in maximum 1-day precipi- tation. . . . .	29
19	Enumeration areas in the 2015 Sierra Leone national census. . . . .	30
20	Nodes with high flood risk, node degree centrality and aggregate failure rate shown in regular scale and log scale. . . . .	32
21	View of nodes in the power network with risk of failure due to floods. . . . .	33
22	Failure rates of all damage states that may occur. . . . .	33

23	Visual representation of the cascading failure that occurs with the failure of individual nodes 125 and 33. . . . .	34
24	Parallel plot showing comparison of impacts between damage states. . . . .	35
25	Parallel plot showing tradeoffs between the selected policies for Damage Scenario 20/66. . . . .	36
26	Parallel plot showing tradeoffs between the selected policies for Damage Scenario 125. . . . .	37
27	Failure rate of nodes with flood risk under future climate scenarios . . . . .	38
28	View of nodes experiencing flood risk under future climate scenarios. . . . .	38
29	Parallel plot indicating estimated change in failure rates of exposed nodes in future time periods under RCP4.5. . . . .	39
30	Failure rates of the top 10 most likely damage states under future climate scenarios. . . . .	39
31	Overlay of December 2017 and 2020 VIIRS-DNB nightlights images in Sierra Leone with the derived power network data. . . . .	40
32	Discrepancies between distribution of population sizes as indicated by the national census and WorldPop estimates. . . . .	41
33	Discrepancies between distribution of poor households representation as indicated by the national census and DHS survey estimates. . . . .	42
34	Discrepancies between distribution of women-headed households representation as indicated by the national census and DHS survey estimates. . . . .	43
35	IDs of nodes on high-voltage line from Bumbuna to Freetown in Sierra Leone. . . . .	59
36	Visual representation of the cascading failure that occurs with the failure of individual nodes 20, 66 and 125. . . . .	60
37	Visual representation of the cascading failure that occurs with the failure of individual node 20 (left) and node 66 (right). . . . .	61
38	Visual representation of the cascading failure that occurs with the failure of individual nodes 20/66 (left) and nodes 20/125 (right). . . . .	61
39	Visual representation of the cascading failure that occurs with the failure of individual nodes 33/125 (left) and nodes 66/125 (right). . . . .	62
40	Distribution of discrepancies between WorldPop and census estimates. . . . .	63
41	Distribution of discrepancies between DHS survey interpolation estimates and census estimates for poor households. . . . .	63
42	Distribution of discrepancies between DHS survey interpolation estimates and census estimates for women-headed households. . . . .	64

---

43	Scatter plots showing change in network performance given variations in transmission line capacitance in each damage state scenario. . . . .	65
44	Scatter plots showing change in network performance given variations in spatial distribution of loads in each damage state scenario. . . . .	66
45	Scatter plots showing change in network performance given variations in transmission line reactance in each damage state scenario. . . . .	67

## List of Tables

1	Impacts for each damage state scenario in the base case. . . . .	35
2	Set of policies that yield best performance per metric. . . . .	36
3	Enumeration of all policies considered in the analysis. . . . .	59

# 1 Introduction

Governments today are faced with rapid population growth and runaway climate change, factors which are linked to increasingly frequent and damaging natural disasters (Bouwer, 2011). Furthermore, urbanization trends have concentrated resources, people and activities in localized areas, in turn magnifying the human and economic costs of disruptions occurring in those areas. Thus, many local and national governments the world over are working to incorporate resilience-building objectives into their policy agendas (UNDRR, 2020).

As part of this initiative, governments must also take assertive action to foster and protect national infrastructure assets, such as those related to transportation, energy, and healthcare. Such infrastructure assets are deemed “critical” when their disruption or destruction “seriously impacts the health, safety, security, or economic well-being of citizens or the effective functioning of governments” (European Commission, 2004). Underfunding, poor planning, and maintenance of infrastructure assets are some of the factors that prevent universal access to reliable basic services (Sheng, Carrillo-Rodriguez, Eun-Young, Perez-Ludena, & Mukherjee, 2007).

Critical infrastructure networks also suffer increasing exposure to rapid-onset climate-related hazards, which can quickly destroy valuable infrastructure assets. A related and increasingly relevant phenomenon is that of cascading failures, which occurs when localized asset damages in a facility or link propagate downstream through the network. This causes a cascade of failures that can incur substantial direct (e.g., damages to property and infrastructure) and indirect (e.g., decline in revenue or wellbeing) losses. The increasing interdependence of national infrastructure systems, defined as “a physical, logical, or functional connection from one infrastructure to another, where the loss or severing would affect the operation of the dependent infrastructure”, exacerbates these cascading risks and amplifies the impacts of a disaster (Toole & McCown, 2008).

Energy infrastructure, which includes electric power generation and distribution systems, is typically considered one of the most important critical infrastructures. This is due to the enabling functions that energy infrastructure provides across all other critical infrastructure sectors. National power transmission systems typically consist of multiple interconnected sub-grids located across a country, enabling the delivery of electricity from generation plants to end-users (Blume, 2016).

The interconnected nature of power networks causes the system to be exposed to high risks of cascading failures. The failure of an individual component in the power network can result in a succession of failures downstream of the network and result in large-scale power outages (North American Electric Reliability Corporation, 2013). This cascade of failures occurs due to various reasons such as line overloads, whereby the load from a failed line is distributed over surrounding lines that may not have the capacity to transmit those loads, thereby triggering further line failures (Koc, Verma, Araujo, & Warnier, 2013). Other reasons for cascading failures include thermal overloads and voltage instability in the power network (Vaiman et al., 2012).

To mitigate these failures, it is essential that the risk profiles of network components are clearly understood such that appropriate risk management strategies can be developed and implemented. Given the mounting incidence of climate-related hazards, an important component of national resilience building is to manage and reduce disaster risk. Floods comprise some of the most frequently occurring and damaging climate-related hazards (Najibi & Devineni, 2018),

while trends in global sea-level rise suggest that the number of people impacted by storm surges may experience a five-fold increase by the 2080s (Nicholls, Hoozemans, & Marchand, 1999).

During flood events, power network components face an elevated risk of destruction, which can trigger or exacerbate cascading failures and result in widespread power outages. Given the central role of energy infrastructure in supporting the functions of other critical infrastructure, failures in the national power transmission network can lower the overall quality of national critical infrastructure. This creates a need to identify parts of the networks which are not only exposed to high flood risk but also pose a high risk of triggering or exacerbating cascading failures.

In many countries, disruptions to the power supply can severely limit the access of millions of people to basic services, which is crucial for creating economic opportunities for the poor (International Labour Organization, 2008). These challenges are exacerbated by unmitigated disaster-related risks in low-income countries, where policy makers must allocate scarce resources to meet multiple urgent development goals. These goals are broadly encapsulated by the Sustainable Development Goals (SDGs) set forth by the United Nations (2015). Disaster events have the potential to incur high damages and losses, thereby setting back progress towards SDGs such as No Poverty (Goal 1) and Affordable and Clean Energy (Goal 7). Understanding and mitigating the disaster risks that compromise the quality of electricity provision is therefore important for the well-being of many.

In many parts of the world, the design process for policy interventions is increasingly supported with data-driven techniques, particularly given the mounting sophistication of data collection and analysis methods. However, many low-income countries lack an established system for collecting and managing data of high quality and coverage (OECD, 2017). This reduces the capacity to inform policy-making with a data-driven understanding and analysis of problem contexts. This challenge may be especially damaging in countries where resources are severely limited. However, rapidly advancing technologies and techniques are making it possible to develop global data sets of increasing resolution and accuracy. Strategic use of such data sets can create opportunities to incorporate evidence-based analysis into the policy-making process in countries where the necessary data is lacking or unavailable. This research thus aims to explore the use of such data sets in understanding flood risk and impacts on a power network.

## 1.1 Research objectives and questions

This section presents the main research objective of this project, which is to develop a method for identifying the power network components that are exposed to flood risk, and how the failure of those nodes may trigger or exacerbate cascading failures within a real-life power network in data-scarce countries. The method will also quantify the impacts of these cascading failures using multiple metrics selected based on technical and welfare considerations.

Given the overarching research objective, the main research question as follows: **How to overcome data scarcity when analysing the impacts of cascading failures in power networks caused by floods?**

Based on the main research question, we formulated the following research sub-questions, which highlight the specific knowledge that is needed to address the main research question:

1. What are the key components characterizing the research problem that can be derived from global data sets?
2. How does the power network respond to a disruption caused by failed nodes in the network?
3. What are the ways to analyse the impacts of cascading failures in the power network?
4. How can the proposed method be used for the analysis of policy interventions?
5. How can the proposed method be adapted to account for uncertain future scenarios?

To begin with, this research first seeks to conceptualize the research problem and to understand which data sets can sufficiently characterize the key components that are required for this analysis. Based on the main research question, these key components are the flood risk, the cascading failures, and the impacts analysis. The data sets must contain sufficient coverage and resolution on the research component it aims to represent. As examples, data should be available for the full geographic extents of the country (i.e., not for one city or state only), and gridded data sets with small cell sizes or neighborhood-level resolution would be favored over the district- or province-level data sets. Once data sets that meet the requirements are identified, they can be collected and processed for analysis.

In formulating the remaining research questions, we adopted an XLRM framework as introduced by (Lempert, 2003). The XLRM framework can be a helpful approach to structure an analysis of a system. It groups the elements of the analysis into four categories, listed as follows:

1. Exogenous uncertainty (X): Events (e.g., climate change) outside of the control of the decision-makers, which may affect the outcomes of the system that the policy maker is invested in. These are referred to as uncertain scenarios in this report.
2. Policy levers (L): Interventions or strategies that policy makers may wish to explore for achieving their goals.
3. System relationships (R): The ways in which elements within the system being analysed relate to and impact one another.
4. Measures (M): Performance standards, or metrics, that policy makers may use to evaluate and rank the desirability of an outcome. Different stakeholders may have varying ideas of what constitutes a favorable or adverse outcome, which can be measured in different ways. It is therefore important, when evaluating the effects of flood risk on power networks, to consider a range of perspectives for measuring those impacts.

The XLRM framework helps to structure the research at hand, with the power network and how it responds to flood risk (in terms of cascading failures) representing the system being analysed. Given this perspective, the subsequent research question seeks to shed insight on the “Relationships” component of the framework. First, a flood risk analysis should reveal which power network components are exposed to the hazard. The failure of these nodes is used as the initial conditions for a cascading failures analysis. These two steps are required for answering the second research sub-question, which aims to develop an understanding of the magnitude

and spatial extent of a cascading failure resulting from one or more isolated disruptions in the power network.

We then move on to addressing the “Measures” component of the framework. Performance metrics, which may be used to quantify the impacts of cascading failures, often form the basis for decision-making and should therefore be carefully selected. Metric selection and impacts quantification will be explored when answering the third sub-question.

The final two research sub-questions aim to show how this method may be adapted to support the policy maker’s endeavor to account for uncertain scenarios (“eXogenous factors”) or to evaluate policies (“Levers”). The fourth sub-question seeks to show how a potential set of interventions to mitigate the impact of cascading failures in the power network can be implemented, tested, and evaluated. In answering the final sub-question, we will show how uncertain scenarios can be taken into account when using this method to analyse the flood risk of the power network.

## 1.2 Research approach

The employed research approaches used to answer the research questions include literature review, modelling and simulation, and case study. A literature review will establish an understanding of extant research and knowledge in the research domain, which informs how the model is conceptualized and implemented. modelling enables the integration of different system processes into a unified framework and facilitates a holistic understanding of those process interactions and responses to changes. This creates the opportunity to simulate the impacts of sets of interventions and subsequently analyse policy performance and trade-offs in a controlled environment. The case study provides an opportunity to apply the model and gain potentially useful insights in a real-life context.

## 1.3 Thesis outline

This thesis is outlined as follows:

1. Chapter 2 of this thesis outlines the literature review and establishes the research gap.
2. Chapter 3 delineates the conceptualization and implementation process used to develop the model. This chapter will also describe the methods for developing policy interventions and scenarios, as well as the experimental approach used to test the interventions.
3. Chapter 4 describes the process of applying the method within the case study location (Sierra Leone) context.
4. Chapter 5 presents the outputs of the model based on the case study location. Model outcomes are presented for the status quo (base case) setting and compared with outcomes that take into account (i) future climate scenarios, and (ii) implementation of interventions. We also present results from a validation and sensitivity analysis in this chapter.
5. Chapter 6 discusses implications of the model outputs, validation exercise, and sensitivity analysis.

6. Lastly, Chapter 7 provides a conclusion summarizing the research findings, research contributions, research limitations, and potential future work.

## 2 Literature Review

The goal of the literature review was to establish an overview of existing research on modelling and simulation of power networks, as related to cascading failures caused by climate-related disasters. For a more comprehensive view on how to study the impacts of natural disasters on power networks, we expanded our search to include models that simulate disruptions not just from floods, but from all climate-related disasters.

### 2.1 Modelling of power networks

A national power network is typically made up of multiple high voltage (more than 110 kV), medium voltage (more than 50 kV), and low voltage (less than 50 kV) transmission grids. These grids are interconnected via transmission substations which step down voltage levels from the higher level to lower level transmission grids. From the low voltage transmission grid, electric power is transmitted over distribution lines to service locations, where it is further stepped down to a voltage level that is suitable for the consumption of end-users (e.g., households and businesses) (Koc, 2015).

Typically, generated electric power is transmitted at high voltage levels from generation plants via transmission substations and transmission lines to end-users. The power flows in a grid in accordance with Kirchoff Laws, which are the set of rules that describe the conservation of current and energy within electrical circuits and which dictate power flow in a network (Blume, 2016). Accordingly, the physical properties of a grid (e.g., impedances, voltage levels at each individual power station, voltage phase differences between power stations and loads at terminal stations) control power flows in the power network.

The occurrence of a disturbance in a power network can initiate a cascading failure, which is defined as “the uncontrolled successive loss of system elements triggered by an incident at any location” (NERC, 2013). Electric power networks typically operate with an  $N-k$  secure criterion, where  $k$  indicates the number of components that may fail without disrupting the functioning of the system (Bienstock & Verma, 2010). However, even within such systems, any of the  $k$  failures may concatenate alongside other unexpected component failures or operational errors, leading to a cascading outage.

Various events can trigger an initial failure of a cascade, such as natural disasters, operational (human) error, or unexpected component failures (e.g., resulting from a lack of maintenance) (Vaiman et al., 2012). During a cascade phase, the power system becomes unstable, as transmission lines are triggered successively in a short time, leading to worsened system instability. This phenomenon typically occurs in a short time period ranging from milliseconds to tens of seconds (Koc et al., 2013).

The above forms the foundation for a vast repository of research on cascading failure and recovery in power networks with a modelling and simulation approach. Models are often used to analyse the cascading process. We reviewed a number of such studies to understand the data inputs that are required for implementing such models. It was found that the most common modelling approaches can be categorized into four types, which are optimal operation modelling, agent-based modelling, network topological modelling, and probabilistic modelling (Wang et al., 2019).

Optimal operation modelling is comprised of mathematical models containing equilibrium equations, constraints, and objective functions, seeking strategies that most effectively allocate resources or reduce load shedding. When the system is interrupted, achieving recovery can be interpreted as an optimization problem to restore the system within a short time while minimizing the load shedding ratio. We found this modelling approach to be unsuitable for this research given the mathematical and abstract nature of the approach, which makes it challenging to model cascading failures for large systems (Wang et al., 2019). Studies employing this approach also do not take hazard risks into account. Instead, network component failures are simulated generally, such as by removing select or random system components and reviewing the resultant impact on the overall system (Arif, Wang, Wang, & Chen, 2017; C. Chen, Wang, Qiu, & Zhao, 2015).

Agent-based modelling (ABM) is a bottom-up approach to simulate the actions and interactions of autonomous agents with the objective of observing the impacts of individual agent behaviors on the system as a whole. ABM focuses on the analysis of the interactions between interdependent entities and systems, allowing for behavioral analysis and simulation of socio-economic activities. The ABM approach can be very useful when classes of agents can be differentiated with sets of decision-making rules that inform interactions with their environment, for example when analysing energy supply chains (S. Chen, Compare, & Zio, 2019) or energy demand dynamics (Bustos-Turu, van Dam, Acha, Markides, & Shah, 2016). However, this approach can be very computationally expensive at larger scales and with a higher number of agents.

This review found that a more suitable modelling approach is network modelling. This approach is based on graph theory, whereby the network topology of the power network is modelled as a collection of nodes (generation, transmission, and distribution stations) and edges (transmission lines). This approach allows examination of the relationship between the topological structure of a power network and its operational performance (Guo, Zheng, Iu, & Fernando, 2017). This approach is based on graph theory, whereby the topological representation of power networks is modelled, and failures within the network are implemented with node or link removal. The impacts of component removal can then be evaluated in terms of topological metrics such as mean path length, clustering coefficients, and node centrality (Buldyrev, Parshani, Paul, Stanley, & Havlin, 2010).

One study that simulates cascading failures in infrastructure systems using networks is that by Zorn, Pant, Thacker, and Shamseldin (2020), where multiple infrastructure systems and their interdependent relations are modelled with a network-of-networks approach. Cascading failures through the networks are simulated with a loop that updates damage states with each iteration until an equilibrium state is achieved. In this study, the simulation of failure propagation is based on the path dependence of connections. For example, if alternate paths exist that are able to maintain the flow of entities between two nodes, it is assumed that no losses are suffered when one of the paths fails.

A different study by He (2018) adopts a similar network-of-networks approach, where infrastructure facilities are connected by links that characterizes the flow of entities (e.g., products, information, and services) as well as functionality dependency matrices. In this study, initially failed components (nodes or links) are identified by combining hazard information (e.g., wind speeds) with fragility curves that characterize the functionality state of each component. Failed components are then removed, and the network topology is updated until equilibrium is reached.

Network modelling can be an efficient and effective method for observing the phenomenon of cascading failures in power networks. However, purely topological models are highly abstract and fail to capture the physical properties and operational constraints of power networks (Cuadra, Salcedo-Sanz, Del Ser, Jiménez-Fernández, & Geem, 2015). As summarized by Guo et al. (2017), power network component failures initiate a process of load redistribution in the system, which leads to overloading of other transmission lines or dynamic instability in generation units, thereby causing a cascading failure. The reviewed studies make clear that cascading failures can be triggered or propagated by factors beyond network topology, and that omitting consideration of these factors can mislead study findings (Wang et al., 2019).

A more realistic cascading failures analysis should include consideration of the physical properties of the network and power flows (Sun, Han, Cao, et al., 2005; ?). A modified topological network modelling approach extends the purely topological models by incorporating non-trivial features, such as power flow distributions and line flow limits. The open-source model MAT-CASC, by Koc et al. (2013), takes into account transmission line capacities and power flow distributions while simulating cascading failures in power networks due to line overloads. Such an approach bears higher fidelity to real-life processes as compared to purely topological network models.

The above studies show that data on the power network topology is required to analyse the occurrence and impacts of cascading failures in the country being studied. Furthermore, as it is important to consider the effects of electrical properties of the network when conducting such studies (Guo et al., 2017; Wang et al., 2019), additional information on network properties (such as component voltage capacities, line limit capacities, and other characteristics) would be required.

## 2.2 Simulation and impacts of climate-related hazards

We further reviewed how the various studies conceptualized and implemented the disruptive event (such as climate-related hazards, which include floods). Many studies adopted a deterministic approach for modelling hazards, such as the study by Cicilio et al. (2020), where a set of links is specified to fail at pre-defined timesteps in order to simulate a hurricane traveling along a coastal area. Zorn et al. (2020) modelled disruptions based on the spatial intersection of infrastructure assets with a predetermined extent of a hazard. Another example is the study by Zhang and Peeta (2011), who modelled generalized failures by reducing the capacities of components within the modelled infrastructure system.

Another approach for simulating failures in power networks due to natural disasters is via probabilistic modelling. This approach entails implementing probabilistic algorithms (e.g., stochastic models) to capture the uncertain, stochastic behavior of climate events and simulate the disruption process of power networks. Probabilistic modelling enables users to evaluate the risk faced by a power network to stochastic weather events and natural disasters. This approach often entails the coupling of hazard intensity data with fragility curves to simulate the probabilistic failure of an infrastructure component.

Fragility curves were initially introduced and developed for conducting seismic risk assessments at nuclear power plants (Kennedy, Cornell, Campbell, Kaplan, & Perla, 1980). Fragility curves quantify the relationship between hazard and impact by mapping the probability of exceeding a particular damage state to a hazard intensity. In a study by (Jeong & Elnashai, 2007),

the authors enumerate three approaches to developing fragility curves: (i) the judgmental approach, where expert judgment is used to inform curve parameters, (ii) the empirical approach, where observational or empirical data is used, (iii) the analytical approach, where structural models are used to evaluate performance limits of the component. The authors also discuss a hybrid approach, which consists of two or more of the three named approaches used in tandem.

One example of a fragility curve developed via a judgmental approach is proposed in Hazards-US (HAZUS), a loss estimation framework for damage to assets caused by natural hazards ([Federal Emergency Management Agency, n.d.](#)). While this framework was first developed for estimating damages due to earthquakes, a series of technical manuals tailored to other hazards, such as hurricanes, floods, and tsunami, have been developed. Of particular interest to this research is the flood technical manual, which contains parameters that inform the damage functions and functionality thresholds for different classes of power network components, in terms of percent damage by the depth of flooding. In this research, the damage state of interest is equivalent to the functionality threshold, exceeding which the infrastructure component is considered to have failed.

As an example of fragility curve application, the model by [He \(2018\)](#) used historical hurricane track data and a wind field model to identify wind speed at every location in the case study. Failures of infrastructure components were then determined with probabilities specified by fragility curves based on wind speeds. A study by [Sánchez-Muñoz et al. \(2020\)](#) used detailed flood maps that contained water depths of each flooded area. They intersected the flood maps with a data layer containing the location of the power network components to identify flood depth at each component. They then connected these flood depths with fragility curves provided by [Federal Emergency Management Agency \(n.d.\)](#) to obtain a probability of failure.

### 2.3 Impact assessments

As the proposed method should enable policy makers to test and evaluate policy interventions, the metrics used to frame the impacts of and tradeoffs between the interventions must be carefully considered. In many of the reviewed power network studies, the performance of the infrastructure system is evaluated based on reliability or resilience metrics. [Clark-Ginsberg \(2016\)](#) describes reliability as a measure of the consistency of the infrastructure to deliver services in the quantity and with the quality demanded by users, and resilience as the infrastructure's ability to recover or adapt quickly to adversity. Therefore, while the end goal of energy infrastructure is to achieve reliability, resilience is the trait required to achieve this end goal.

The reliability and resilience metrics are often quantified using the loss of load and time to recovery as metrics. Loss of load is one of the most direct ways of measuring the impact of a cascading failure ([Vaiman et al., 2012](#)). Another common metric to quantify power network performance is the amount of power delivered by the system ([Ayyub, 2014](#)). In the context of this research, an intuitive corresponding metric would then be the amount of power *not* delivered due to a cascading failure. Among the reviewed studies, several authors employed reliability metrics to evaluate the impacts of disruption on a system, such as the System Average Interruption Duration Index (SAIDI) or the System Average Interruption Frequency Index (SAIFI). Many optimal operation models had the recovery objective incorporated into the objective function of the optimization model, seeking to maximize post-disruption picked-up loads or minimize service restoration time. Other studies include more detailed performance

assessments, such as that by [Cicilio et al. \(2020\)](#), who plotted a resilience trapezoid using the loss of load over time, outlining three system states across the trapezoid: disturbed, post-disturbance degraded, and restorative states. The area under this trapezoid is taken as a quantitative indicator of system resilience.

Using the loss of load to quantify the impact of a cascading failure may be viewed as a utilitarian choice, defined as the option that “yields at least as high a sum total of utilities as any other alternative act” ([Sen, 1979](#)). This is because the loss of load as a metric does not inherently differentiate between those impacted, thereby disregarding the distribution of costs and benefits among recipients. As this research is aimed at supporting the decision-making process of policy makers, we consider that the method should allow policy makers to take other considerations into account.

One such consideration is social welfare. Various studies have shown that power outages disproportionately affect the socio-economically disadvantaged. For example, a study on the impacts of a one-month-long power outage in Tanzania revealed adverse outcomes in terms of maternal stress, leading to lower-than-average birth weights of newborns ([Burlando, 2011](#)). A different study by [Kesselring \(2017\)](#) discussed the inherently politicized nature of infrastructure access and how power outages exacerbate social inequalities, with a focus on mining towns in Zambia. More generally across the continent, [Aidoo and Briggs \(2019\)](#) discuss how the poor disproportionately bear the brunt of power outages in Africa.

Thus, the importance of assessing the social dimension of the impacts resulting from cascading failures in power networks is clear. We found that some of the reviewed studies included assessment of disruption impacts on populations or end-users of basic service facilities. The study by [He \(2018\)](#) assessed impacts of the cascading failures on critical end-user facilities (e.g., hospitals) based on facility proximity to the failed infrastructure. [Zorn et al. \(2020\)](#) estimate the number of users relying on a service point based on a Voronoi tessellation method, which was used to calculate the total number of users affected by a disruption. However, none of the reviewed studies on power network disruptions included consideration of the socio-economic vulnerabilities of those affected.

### 3 Method Implementation

This chapter describes the proposed method used to answer the research questions outlined in Chapter 1.1. This chapter identifies the key components of the research problem which are required to develop a conceptual representation of the research problem.

For each component, we discuss the required information vis-à-vis available global data sets and outline the strategies used to manage mismatches between the two. This is followed by a discussion on the methods used to process the data for implementation into the MATCASC model. The chapter closes with examples of additional analysis that can build upon the proposed method. The following diagram (Figure 1) presents a broad overview of the method.

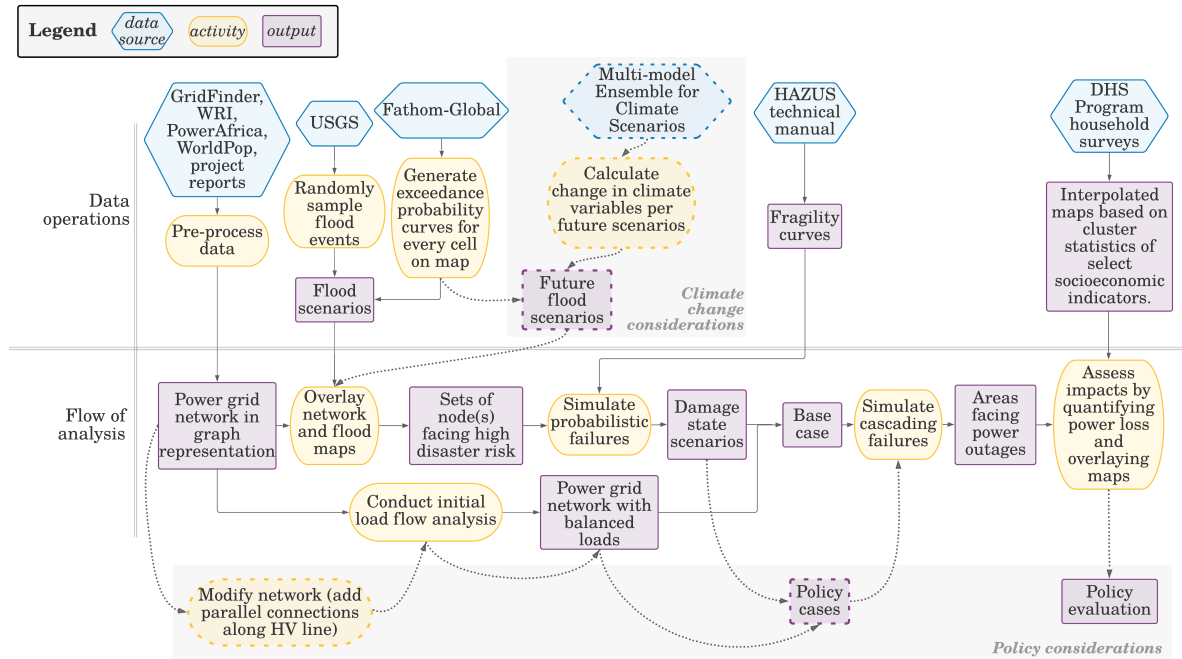


Figure 1: Summary of data sources, data processing activities and analysis process.

#### 3.1 Power network representation

This sub-chapter presents the process for generating a representation of the power network of a country that is required for the cascading failures analysis.

##### 3.1.1 MATCASC model and requirements

This research makes use of the open-source MATCASC model, which is openly available on GitHub.<sup>1</sup> MATCASC is a MATLAB based package built upon MATPOWER, a power flow solver for MATLAB users (Zimmerman, Murillo-Sánchez, & Thomas, 2010). MATCASC simulates the cascading effects of failures resulting from line overloads. As the cascade of failures

<sup>1</sup><https://github.com/trivikverma/MATCASC/>

due to line overloads occurs in mere seconds, the time horizon for the simulation spans across the moments of a failure occurrence.

To complete this research, we converted the MATCASC package from MATLAB into the Python programming language, incorporating the use of modules from the PYPOWER library, which is a port of MATPOWER into Python. This was done to simplify the adaptation of MATCASC inputs and outputs into the geographic data sets required for this analysis.

The model implements a DC power flow analysis approach to estimate power flow values across the network. In contrast to AC power flow analysis, the DC analysis approach takes into account active (real) power flows only, does not consider line resistance, and assumes a flat voltage profile as well as negligible voltage phase differences. Thus, the cascading failure simulation accounts for electric power flows in the network, which is estimated based on real power flows and voltage angles at network nodes. The simulation also takes into account the physical properties of the grid, such as transmission line capacities and reactances (Koc et al., 2013).

Simulation of transmission line failures in MATCASC is based on (i) line maximum capacities, and (ii) line admittances. The maximum capacity of a line is proportional to its initial loading level by way of a tolerance parameter, alpha ( $\alpha$ ). A tolerance parameter of 1 assumes that the network is fully loaded in the initial condition, while a higher tolerance parameter assumes that the network has excess capacity to absorb redistributed loads (Koc, 2015). Meanwhile, line failures are implemented by setting the corresponding line admittances to zero, thereby eliminating all potential flow through those lines. In the event of line failure, power flows will be redistributed across the surrounding available lines. If the redistributed power flow across a line exceeds the pre-specified maximum capacity of the line, another line overload occurs and results in further line failures. This process is reiterated until equilibrium is reached (Koc et al., 2013).

The inputs required to analyse cascading failures in MATCASC are (i) a casedata file representing the topology, electrical properties, and load distribution of the power network, (ii) the tolerance parameter ( $\alpha$ ) for the transmission lines, and (iii) the removal strategy for determining the initial line threats in the network (Figure 2). As this research aims to analyse the flood risk of the power network, this model was adapted such that the failure of a node (or set of nodes) exposed to disaster risk are directly input as initial line threats in the model (see Chapter 3.2).

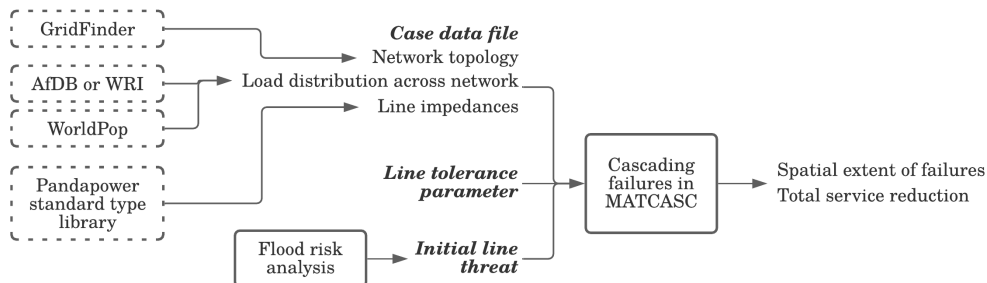


Figure 2: Summary of inputs and outputs of MATCASC as adapted for this research

In summary, the model requires data on power network topology, transmission line properties, and network loading profile in casedata format. The objective of this network cleaning

exercise was to obtain a set of nodes that represent the power generation, transmission, and distribution stations, as well as a set of edges representing the transmission lines connecting those stations. Information on the loads and voltage angles at network nodes and the physical properties (e.g., resistance and reactance) of the transmission line should be included. Furthermore, this information should be geographically explicit so that the disaster risk of network components can be accounted for. However, detailed power network data is often unavailable or has restricted public access for reasons such as security-related concerns. To address this hurdle, we explored the following global and regional data sets:

1. GridFinder, for the derivation of power network topology<sup>2</sup>
2. Global Power Plant Database by the World Resources Institute (WRI), for geographic coordinates and generation capacities of power plants<sup>3</sup>
3. Power Africa, an open data initiative by the African Development Bank (AfDB), for geographic coordinates and generation capacities of power plants<sup>4</sup>
4. WorldPop (population counts), for the estimation of load distribution across the network<sup>5</sup>

### 3.1.2 Power network processing

GridFinder consists of an open and global data set derived from a methodology that utilizes algorithms in machine learning and geospatial data analysis, satellite imagery, and known network data to generate a composite map of a connected power network (Arderne, Zorn, Nicolas, & Koks, 2020). We used GridFinder’s vectorized predicted distribution and transmission line network to develop a graph representation of the high-voltage and medium-voltage grid. Given the lack of reliable data on the low-voltage and distribution transmission networks, only medium- and high-voltage (MV/HV) transmission lines are modelled.

Several steps were taken using Python and QGIS to clean and simplify the GridFinder vector data representing the MV/HV transmission lines. The vector data is first clipped using a national boundary shapefile to obtain only the transmission lines within the country of interest and subsequently converted into a NetworkX graph object (Hagberg, Schult, & Swart, 2008). The resultant graph consists of edges with numerous junctions, and nodes at each edge junction. This resulted in many nodes in close proximity of each other (for example, Figure 3, left), indicating that further network simplification was required for the removal of extraneous nodes.

To achieve this, the largest fully-connected transmission network was first obtained by removing stand-alone network segments. Subsequently, we streamlined edge junctions and collapsed close-proximity nodes (i.e., within a specified distance threshold) into single nodes to obtain a simplified network (Figure 3, right). Nodes are then placed at network intersections and termination points in the final simplified graph as load consumption nodes.

---

<sup>2</sup>Available at <https://gridfinder.org/>

<sup>3</sup>Available at <https://datasets.wri.org/dataset/globalpowerplantdatabase>

<sup>4</sup>Available at <https://powerafrica.opendataforafrica.org>

<sup>5</sup>Available at <https://www.worldpop.org/project/categories?id=3>

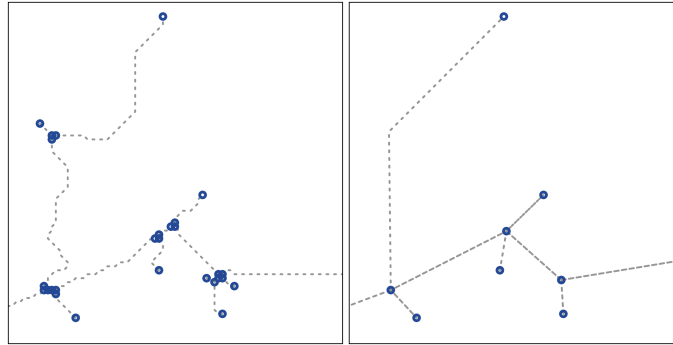


Figure 3: Demonstration of input (left) and output (right) of network simplification process.

### 3.1.3 Power supply and consumption

To incorporate power generation resources, both WRI and AfDB host data sets that contain a list of power plants (and the associated geographic coordinates and generation capacities) in countries globally and in Africa respectively. Based on our observations, the completeness of each data set varies from country to country and may contain some overlap. The data sets may be used to supplement each other, and the list of identified power plants was added to the network as generator nodes. In this research, the total available power supply is modelled as equivalent to the total consumption in order to simulate peak load conditions (e.g., an overloaded system with little excess capacity).

The GridFinder data set further includes a binary raster highlighting locations predicted to be connected to the national transmission grid. This raster was used to identify the areas that obtain electricity through the national transmission system, and which therefore stand to be impacted by cascading failures in the network.

To distribute power demand across the network, a hexagonal grid is first generated and overlaid over the country extents. The hexagonal grid was selected (instead of a square grid, for example) as studies have shown this method to yield increased sampling accuracy (Birch, Oom, & Beecham, 2007). This cell grid is overlaid with the GridFinder raster data identifying areas that receive electricity from the power transmission grid. Hexagon cells that do not intersect with the electrified areas or are far from the MV/HV transmission line are subsequently filtered out.

The remaining hexagon cells are then clustered into “load centers” that represent the lower voltage transmission grids consuming power transmitted from the HV/MV substations represented in the model. As lower voltage power networks often receive power from higher voltage substations, the clustering is implemented to aggregated and designate the areas consuming lower voltage power to a MV/HV source. The clustering process consisted of designating the hexagon cells to the closest node on the simplified network based on network topography and criteria such as the cluster designation of neighboring cells and the shortest distance of the cell to a node.

It is also necessary to determine the distribution of power consumption across the grid. Given that we were unable to obtain any data on spatially disaggregated load consumption, we assumed that the load distribution follows the distribution of population across the country.

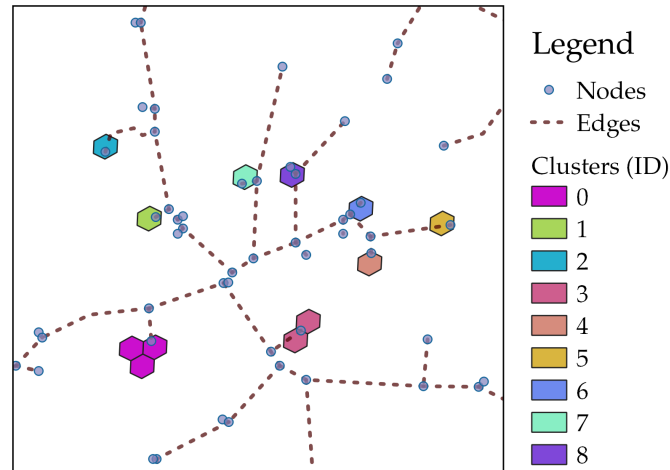


Figure 4: Clustering of hexagon cells into clusters.

To obtain population distribution across the hexagon cells, we used the global WorldPop data sets on population counts by [Lloyd, Sorichetta, and Tatem \(2017\)](#). Weights were assigned to each hexagon cell given the population size in each load center. The assigned weights sum to 1, which represents the total load consumption from the transmission grid.

### 3.1.4 Transmission line properties

Information on the transmission line properties is also required as inputs into the MATCASC model. Barring the availability of detailed country-specific data on power transmission lines, approximations may be made using standard transmission line types included in the Python package, Pandapower ([Thurner et al., 2018](#)). Pandapower is a power flow solver that comes with a standard type library containing predefined parameters for standard power network components including transmission lines. These predefined parameters are defined for a range of line ratings, conductors, and cable configurations, and may be selected based on higher-level information on transmission lines installed in the country of interest.

With the network topology in place, the Python library PyPSA was used to conduct an initial load flow analysis in order to balance the loads across the network and determine the phase angles at all nodes across the network ([Brown, Hörsch, & Schlachtberger, 2018](#)). A load flow solution reflects a steady-state condition of an undisturbed power network, and in this research, represents the initial condition of the network just before the cascade occurs.

The above process results in data on the topology and load distribution in a power network of a country. This data may then be subsequently processed into a casedata format to be input into the MATCASC model.

## 3.2 Flood risk analysis

Flood-plain maps can be used to represent the spatial distribution of a flood hazard, demonstrating the intensity of a flood (e.g., flood depth) and their associated return period. The

return period defines the recurrence interval of an event, also known as the average time between flood events. The higher a return period, the lower the probability of the event occurring, and (typically) the higher the intensity of the event. This research thus uses flood plain maps that indicate the estimated flood depth to which each power network component is exposed.

Fathom-Global 2.0 is the global data set used as a source of high-resolution global flood data (Sampson et al., 2015). The method makes use of satellite imagery as well as data on rainfall, hydrography, urbanization, elevation, and vegetation as inputs for a hydraulic model that produces global flood maps with a resolution of 90m. The flood maps are available for a total of 10 return periods, which are the 5-, 10-, 20-, 50-, 75-, 100-, 200-, 250-, 500-, and 1000-year return periods. Each map consists of a cell array making up a national grid of water depths given the specified flood event. The maps are available for both fluvial and pluvial floods, which indicate flooding caused by overtopping rivers and by extreme local rainfall respectively.

For both fluvial and pluvial flood maps, an exceedance probability curve was generated for each cell in the map by linearly interpolating between the 10 available data points (Figure 5). This allowed the flood heights to be sampled for a broad range of flood events. We further assume that there is a perfect correlation between all cells in a river basin. For example, the flood heights resulting from a 1-in-38 year return period event can be obtained by identifying the flood height corresponding to a value of  $1/38$  on the exceedance probability curve for every cell in that river basin.

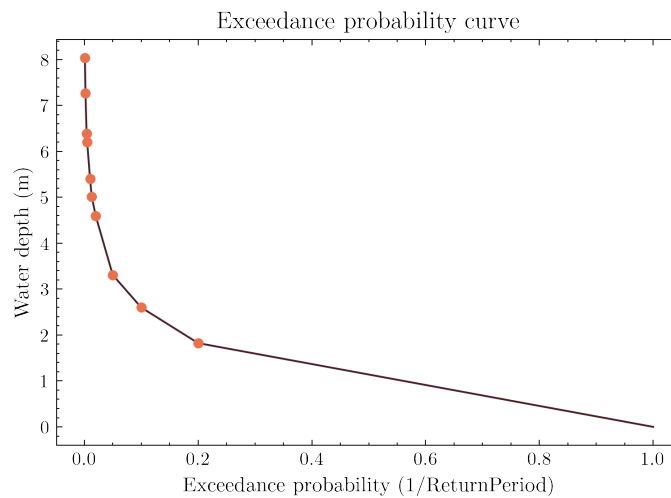


Figure 5: Example of a curve relating exceedance probability to hazard intensity (flood height).

These flood maps represent flood depths across the country in the event that the entire country is simultaneously inundated at the same flood intensity. It must be considered that this scenario is unlikely to occur. Typically, a fluvial flood would take place when a river overtops its banks and water spills onto the surrounding floodplains. Thus, the floods in an area are typically driven by the river basins (drainage sheds) that the area falls within (Verwey, Kerblat, & Chia, 2017). A more realistic scenario would consist of a different flood event occurring in each river basin (with different flood intensities between the river basins) at a single point in time.

A method to generate more realistic flood scenarios would be to segment the country of interest according to the existing river basins. For this purpose, a global data set from the

United States Geological Society (USGS) HydroSHEDS database identifying river basins may be used (Lehner, Verdin, & Jarvis, 2008). The HydroSHEDS data set was a starting point to map the river basins in a country, following which flood scenarios can then be generated by assigning different flood events (i.e., exceedance probability) to each river basin and drawing the corresponding flood heights for all cells within.

Latin Hypercube Sampling (LHS) was used to define flood events for each river basin within the country of interest. LHS is a random sampling method for Monte Carlo-based uncertainty quantification that partitions the sampling region and samples across each of those partitions equally (Helton & Davis, 2003). This method for generating flood scenarios assumes that the river basin flood events are mutually exclusive and independent of each other. Given the specific flood event occurring in a river basin, flood heights for both pluvial and fluvial floods for grid cells in the river basin are drawn. This assumes that these flood events occur simultaneously and with the same exceedance probability. The higher flood height is then taken as the occurring flood height in that grid cell. This process, depicted in Figure 6, results in maps that represent the flood heights across the country under the specified flood scenarios.

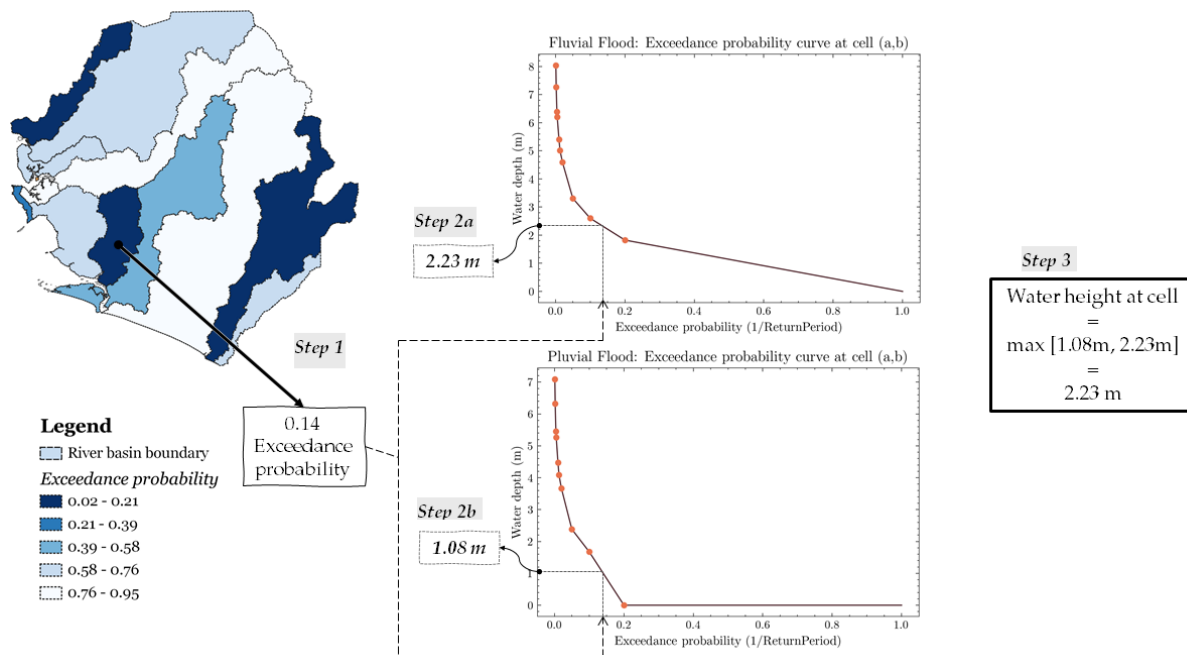


Figure 6: Process for identifying a grid cell flood height for a given a river basin flood event.

Subsequently, we analyse the flood risk of the power network in order to identify potential damage states. A damage state reveals the post-hazard condition of the network, highlighting the individual nodes exposed to flood risk and their rates of failures. It is also possible for multiple nodes to fail simultaneously, in which case the damage state consists of the set of nodes that fail after a hazard event. To generate these damage state scenarios, the flood maps are overlaid with the power network to determine the flood heights at each network component in each flood scenario. A buffer with a 50m radius around each node was created, and the maximum flood height over the 100m-diameter area is drawn (i.e., as opposed to drawing the flood height at a single point location) (Figure 7). This was implemented as a means to account for the uncertainty in the exact substation location and to address the fact that the substations are indeed spread out over an area larger than a simple point location.

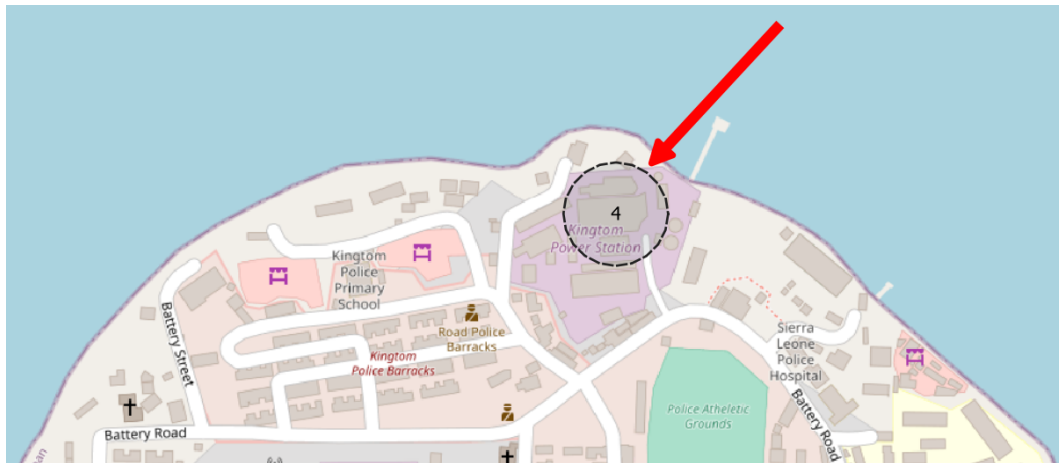


Figure 7: View of network node with a 100m-diameter buffer, representing the Kingtom generation station in Freetown, Sierra Leone.

Next, fragility curves based on the [Federal Emergency Management Agency \(n.d.\)](#) manual are used to identify the probability of failure given the flood heights. The HAZUS manual indicates a functionality threshold of 4 ft. for all electric power network components, with various damage states (enumerated in percent of damage) up until a flood depth of 10 ft. The fragility curves are thus defined based on the HAZUS depth-damage data.

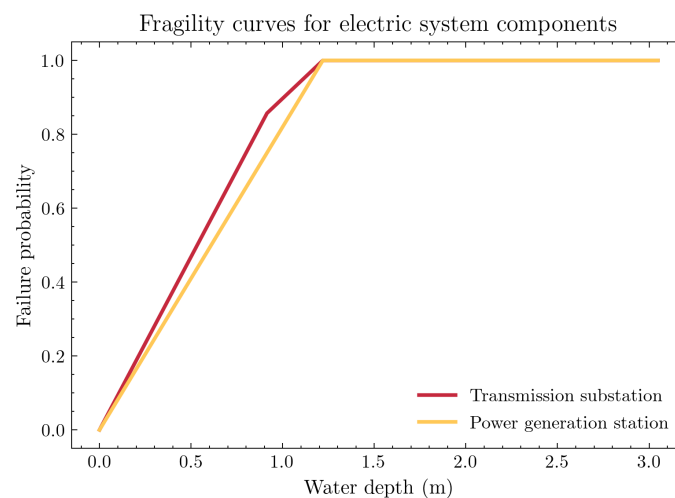


Figure 8: Fragility curves approximated from depth-damage values for electric system components. The functionality threshold is at a 4 ft. (1.2192m) water depth.

Failure probabilities were then evaluated 1000 times for each flood scenario in order to identify the set of node(s) that fail, as well as their rates of failure. The rate of failure of a node is used as a proxy for the level of risk of the node. The set of nodes are thus defined as the damage state scenarios, and transmission lines directly connected to components that face any risk of failure due to floods can then be input into the cascading failures model as the initial threatened lines (Figure 9).

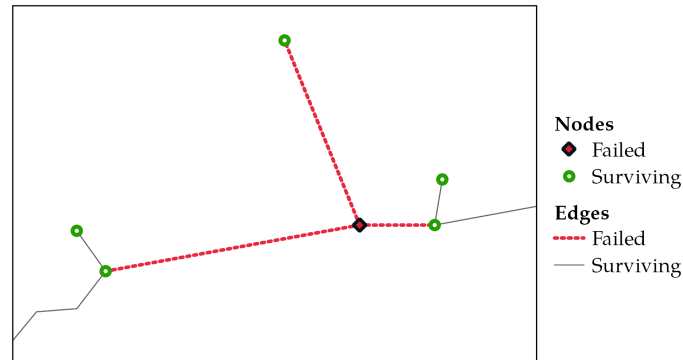


Figure 9: Lines directly connected to a failed node are indicated as initial line threats.

### 3.3 Impacts quantification

The impacts of power outages are often measured in the size of the service reduction (i.e., total power lost). However, as discussed in Chapter 2.3, power outages inflict differentiated impacts across a population, often resulting in worse outcomes for the already disadvantaged. Accordingly, to provide a more holistic evaluation of proposed policy interventions, socioeconomic indicators on gender equity and poverty are used to identify the number of vulnerable households affected by a power outage.

MATCASC provides modules that empirically quantify grid losses in terms of power demand not met and the links that fall out of service. This research expands upon the available MATCASC impact quantification methods to incorporate the assessment of geographically-linked socio-economic impacts. Based on the outputs of the MATCASC model, nodes that lose access to the power supply can be identified. Given the geographic nature of the model inputs, the spatial extent of the areas that experience the power outage can be mapped. Local characteristics of the areas that suffer power outages may then be identified. For example, the size of the population impacted can be quantified, alongside socio-economic characteristics such as the level of poverty or gender equity in those areas.

A global data set that can be used to generate higher-resolution geodemographic information is that provided by the United States Agency for International Development (USAID) Demographic and Health Survey (DHS) program<sup>6</sup>, which makes available survey data covering a broad range of household indicators and statistics related to healthcare, accessibility to services, poverty, and so on. The data set consists of individual and household survey data, aggregated into location clusters tagged with location coordinates across the country.

As demonstrated in past reports by ESCAP (2019) and ESCAP (2020), as well as in the forthcoming report by ESCAP (2021), statistical indicators on a cluster level can be derived from the individual and household survey data. As an example, this study makes use of two survey responses related to socioeconomic vulnerability: (i) the wealth level of the household, and (ii) the gender of the head of the household. Cluster-level statistics are calculated as the number of poor and women-headed households divided by the total number of households per cluster. In accordance with the method demonstrated by ESCAP, these values are then interpolated using Empirical Bayesian kriging (EBK), a geostatistical interpolation method

<sup>6</sup>Available at <https://dhsprogram.com>

(ArcGIS, 2013; Krivoruchko & Gribov, 2019) to generate maps representing the distribution of those indicators across the country. Using the WorldPop population counts in each cluster suffering a power outage, we can then estimate the total number of individuals in poor or women-headed households that are impacted by a cascading failure.

### 3.4 Other considerations

The method described thus far lends itself to other considerations that can support policy-making. Two such considerations are: (i) the performance assessment of policy interventions that can improve network resistance to cascading failures, and (ii) the consideration of a future uncertain scenario (e.g., climate change) impacts on flood risk of the power network.

#### 3.4.1 Policy evaluation

The proposed method should help policy makers evaluate a potential set of strategies, and eventually identify viable options for more comprehensive consideration. Various policy interventions may be implemented to manage flood risk in the power network. Three determinants of grid capability may be considered, which are physical durability, operational versatility, and rehabilitation capacity (Jufri, Kim, & Jung, 2017). Strategies for operational versatility of the grid are most in line with the selected modelling approach. Such strategies include measures such as creating network redundancies by providing alternative lines to those in areas facing high disaster risk.

To demonstrate an example of how such interventions can be tested in this model, this study considers the impacts of implementing network redundancies as an approach to strengthen the power network. Specifically, the network graph is modified to include parallel links added along the segments of the network. The modified network is then processed using the same network as described in this chapter and transformed into casedata format for input into the MATCASC model. Policy performance can then be compared using the proposed impact assessment method against the performance of the modified network against that of the base case (no policy) network.

#### 3.4.2 Climate change impacts

The research also proposes a method for analysing the flood risk of a power network, which can be supplemented by consideration of future uncertain scenarios. In this research, we consider climate change as an example. We do this by evaluating the rate of change in future projections of flood-related climate indicators. One such indicator is the change in short-duration extreme rainfall events (e.g., maximum daily rainfall), which is typically linked to the occurrence of floods (Masereka, Ochieng, & Snyman, 2018).

The Climate Change Knowledge Portal created by the World Bank serves as a repository for comprehensive global data sets on historical and future projected climate indicators.<sup>7</sup> The future projections data sets are generated from an ensemble of global climate models and are segmented

---

<sup>7</sup>Available at <https://climatedata.worldbank.org/CRMePortal/web/water>

into four Representative Concentration Pathways (RCPs), each indicating different scenarios for greenhouse gas emissions and atmospheric concentrations, air pollutant emissions, and land use across four time periods (2020-2039, 2040-2059, 2060-2079 and 2080-2099) (*Climate Change Knowledge Portal*, n.d.). These data sets are of relatively coarse resolution (approximately 100km cells) compared to the Fathom-Global flood maps (approximately 90m cells). Figure 10 shows one such data set for the average maximum 1-day precipitation in 2080-2099 under RCP4.5 scenario.

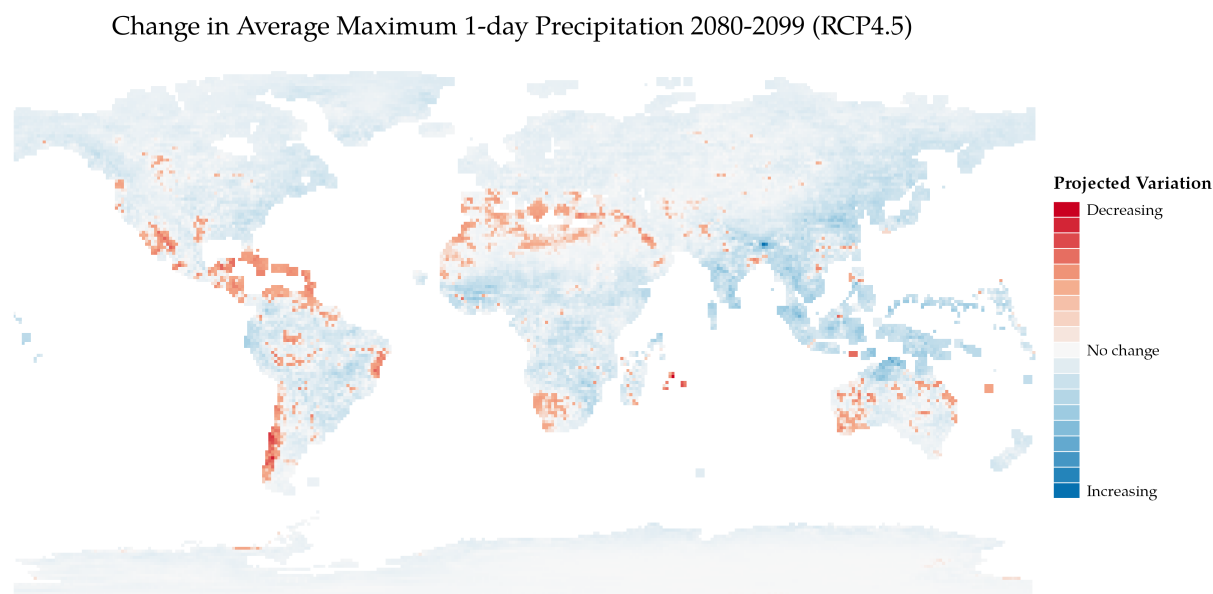


Figure 10: Projected change in average maximum 1-day precipitation in the 2080-2099 time period under an RCP4.5 scenario. Data source: Climate Change Knowledge Portal

To demonstrate this approach, future multi-model ensemble projections for the average largest 1-day precipitation is taken for RCP4.5, an intermediate emission scenario. As we did not have access to base case values for current extreme rainfall, we assumed that the current indication of average precipitation is aligned with the closest time period of 2020-2039. Thus, the rate of change in this indicator is calculated by comparing 2040-2059, 2060-2079, and 2080-2099 precipitation values to the 2020-2039 scenario. The scenario data is first resampled and clipped such that the resolution and extents are consistent with the Fathom-Global maps. Subsequently, for each grid cell, we calculate the rate of change in extreme rainfall for future time periods starting 2040, 2060, and 2080.

The calculated rate of change is used as a multiplier for adjusting the flood heights of the Fathom-Global maps and the subsequent modification of the grid cell exceedance probability curves. Using the same river basin flood scenarios, flood maps that reflect potential future climatic conditions can then be generated. Using these maps, the same analysis can be executed to identify a corresponding set of damage states that reflect the flood risk of the power network. Furthermore, variations in the level of flood risk under the future time periods can be assessed.

## 4 Case Study Application

This chapter demonstrates the application of the method described in chapter 3 to the case study location of Sierra Leone. We begin with a brief overview of the country, followed by a demonstration of how the use of global data sets may be complemented with local data sets to improve the data inputs generated for this study.

### 4.1 Country overview

Sierra Leone has a population of 7.4 million, and at a geographic extent of 71,740 sq. km., is the fifth smallest country in West Africa (BBC, 2018). The country is administratively divided into 4 provinces, 14 districts, 167 chiefdoms, and 1316 counties. According to UNDESA estimates, 42% of the population in Sierra Leone resided in urban areas in 2018. This estimate is projected to increase to 47% by 2030 and 59% by 2050 (UNDESA, 2018). Sierra Leone faces a swathe of development challenges, including poor human capital outcomes, low life expectancies, and widespread poverty and inequality (World Bank, 2019). From 1991 to 2001, the country suffered a civil war that severely damaged the country's physical infrastructure, particularly in the electricity sector.

One of the major binding constraints to growth and poverty reduction in Sierra Leone is a lack of reliable and affordable electricity supply services (World Bank, 2019). Sierra Leone has one of the lowest electricity access rates in the world. According to a World Bank report, only 17% of the total population in the country had access to electricity (Kojima & Trimble, 2016). When taking poverty into account, only 8% of the total poor population had electricity access. While the exact estimate remains unknown, households, businesses, and basic service providers also receive electricity from private diesel generators, privately operated renewable energy-based mini-grids, and home solar photovoltaic products in individual households (ESMAP, 2019).

Beyond the low coverage of electricity provision, the power supply is also inadequate and unreliable, constituting a major barrier to the country's economic recovery and poverty reduction ambition (International Development Association, 2020). The World Bank Enterprise Surveys polled 152 private firms in Sierra Leone and found that they suffered losses on average 11.2 percent of revenue as a result of unreliable electricity services, as compared with the average of 5.3 percent in Sub-Saharan Africa (World Bank, 2017). The electricity service of the main grid has improved to an average of 18 hours per day, although supply interruptions frequently occur due to planned and unplanned outages of generators, transmission lines, and the distribution network (IDA, 2020).

The currently installed generation capacity connected to the main grid is about 104 MW, including a 50 MW hydropower generation plant (Bumbuna) constructed in 2009. However, the total available generation capacity is often lower due to insufficient water supply at Bumbuna dam and inoperable power generation units due to poor maintenance (World Bank, 2020). Sierra Leone's main power network is made up of a 161 kV radial single circuit transmission line connecting the hydropower plant at Bumbuna to the distribution network in Freetown, and nearly 1,000 km of LV lines in poor conditions.

A hazard profile presented in the Hazard And Risk Profile Information System – Sierra Leone (HARPIS-SL) categorized floods as the most high-frequency hazard in Sierra Leone

(*Sierra Leone Hazard Profile, n.d.*). The flood exposure assessment by HARPIS-SL identified the impacts of floods on the most affected segments of society, including the population, housing sector, as well as education and health infrastructure. However, this assessment did not evaluate the impacts of such hazards on energy infrastructure.

## 4.2 Sierra Leone power network

Using an administrative boundary shapefile of Sierra Leone, the GridFinder global data sets indicating the topology of the transmission network and locations of electrified areas were clipped to filter for data within the country extents only. The unprocessed data for the network is shown in Figure 11.

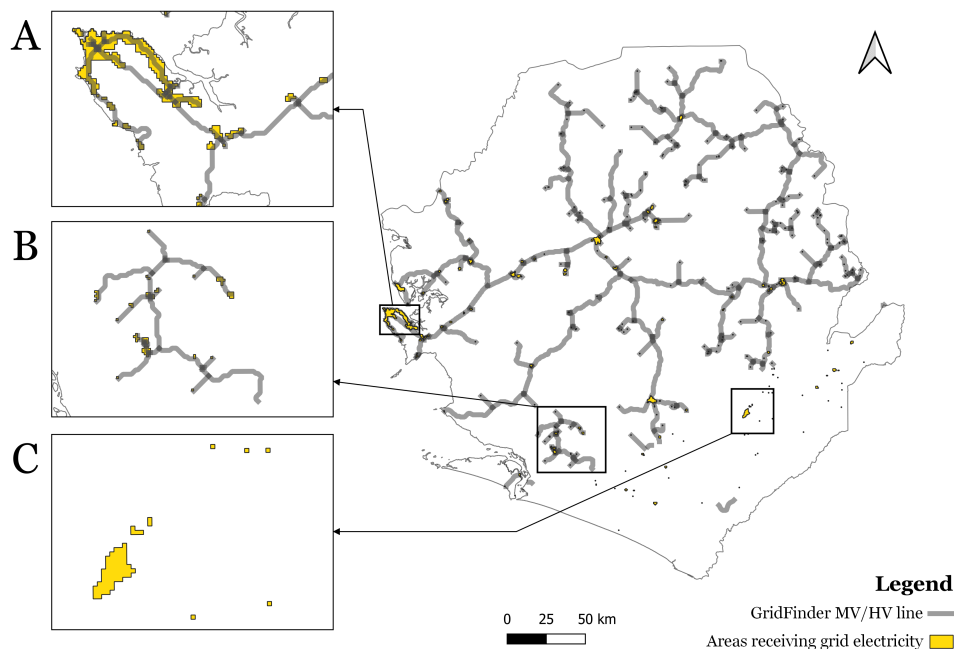


Figure 11: Overview of simplified GridFinder data for Sierra Leone. Inset A shows the transmission line and areas estimated to be connected to the grid in the Western Area. Inset B shows a stand-alone power network. Inset C shows areas estimated to be receiving electricity via lower capacity transmission lines.

Using the NetworkX package in Python, the transmission line vector was converted into a graph object and all stand-alone network components were removed, maintaining only the largest connected network. Subsequently, the network was simplified by merging neighboring nodes located within a 1km distance of each other. This distance threshold was selected based on the assumption that high and medium voltage transmission substations are not expected to be located within 1km of each other. This reduced the number of nodes from 432 to 153 (Figure 12).

We reviewed both the WRI and AfDB data sets for power generation data. It was found that the AfDB data on Sierra Leone was more complete than that by WRI, containing locations and generation capacities of 3 additional power generation plants on top of the 3 plants listed

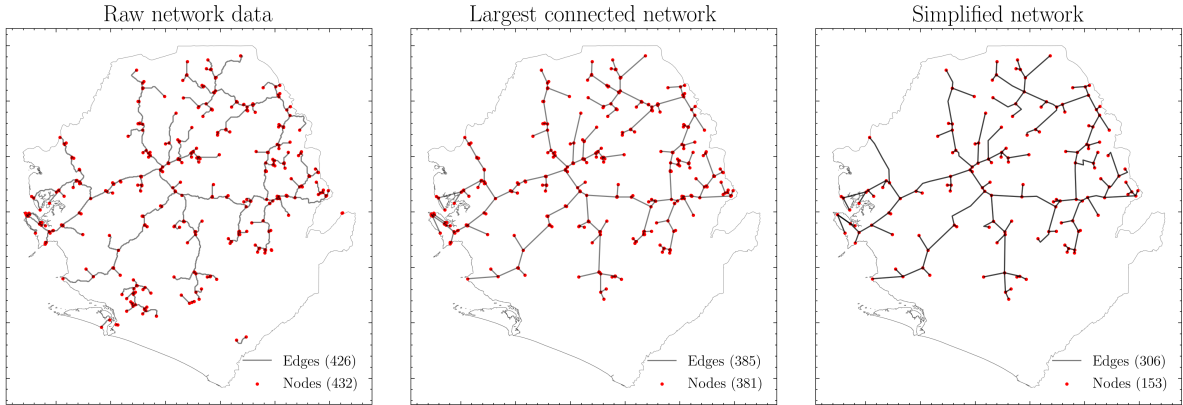


Figure 12: Overview of GridFinder network cleaning process.

in the WRI data set. It was found that 1 of the 6 listed power plants is located in Bonthé, supplying a stand-alone portion of the grid that was omitted from the network in the previous step. This power plant was therefore removed from the list, with the remaining 5 power plants added to the network as generator nodes.

To define the load consumption nodes, the clustering process as described in Chapter 3 was implemented, and the process was visually summarized in Figure 13. The population counts in each cluster of hexagon cells were determined with the WorldPop data set and were used to define load consumption weights in each cell by dividing the population in the cluster by the total population in all clusters. The clusters are represented in the network by either (i) designating the network node intersecting with the cluster as the load consumption node, or (ii) adding the cluster centroid as a new node and establishing a connecting edge to the nearest point on the network. The total generation capacity from the 5 power plants included in the network are divided among all load consumption nodes based on population-derived weights.

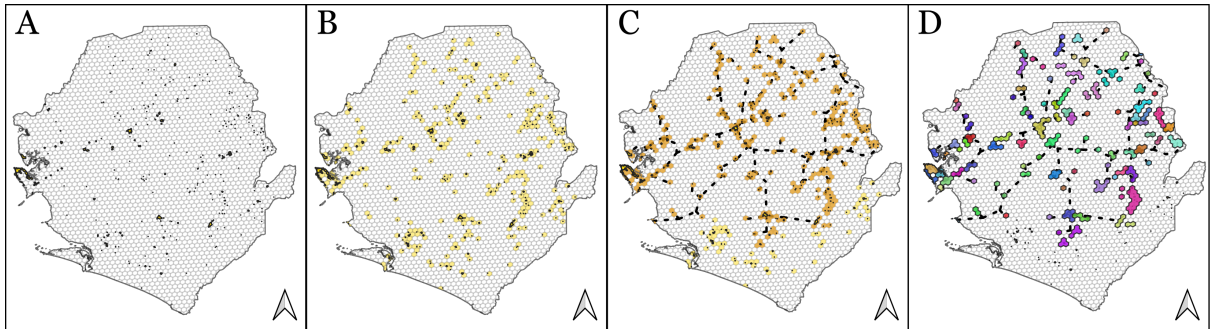


Figure 13: Process of generating, filtering, and clustering hexagon cells. (A) Grid of hexagon cells overlaid with a map of Sierra Leone. (B) Only cells intersecting with denoted electrified areas are kept. (C) Only hexagon cells in proximity of the MV/HV transmission line are kept. (D) Hexagon cells are clustered into 91 load consumption nodes.

The subsequent step was to determine the voltages of the system components. This step was achieved by examining various context-specific sources of information such as past project reports and government websites. It was gathered that the construction of the Bumbuna Hydropower Plant project was accompanied by a 161 kV transmission line was constructed from Bumbuna to Freetown (SEFA & AfDB, 2019). This was confirmed by an Economic Commu-

nity of West African States (ECOWAS) data set<sup>8</sup>, indicating the line extents of existing and future high voltage transmission lines. It was also surmised from other project reports that the medium voltage substations in the national power transmission grid in Sierra Leone comprises 33 kV substations only (EDSA, 2019; MoE, 2017).

To implement the above information, we overlaid the existing high-voltage transmission line (i.e., the 161 kV line from Bumbuna to Freetown) from the ECOWAS data set with the GridFinder transmission line data. The overlapping lines were tagged as 161 kV, while the remaining lines were assigned voltages of 33 kV. Other data sources were used to inform the network topology. For example, the Bo-Kenema power network (as shown in Figure 14, inset C) was manually added into the network based on existing project reports (Ministry of Energy, 2017; AfDB, 2021). The nodes and edges of the processed network are shown in Figure 14.

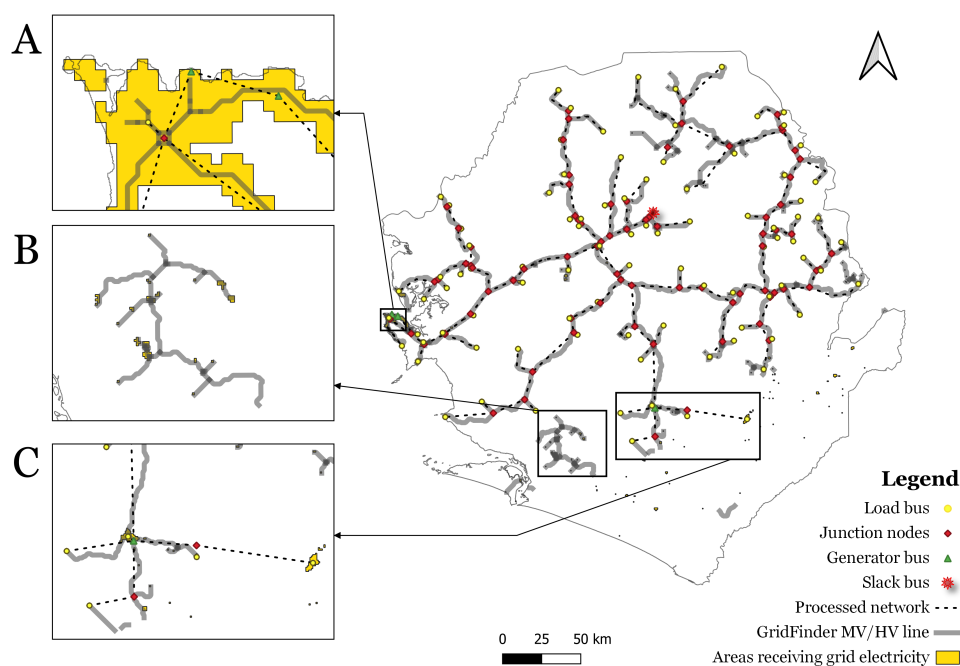


Figure 14: Processed network data for Sierra Leone. Inset A shows the simplified network edges in Freetown. Inset B shows the stand-alone network omitted from the modelled network. Inset C shows the power network extended to represent the Bo-Kenema transmission line.

For the definition of transmission line properties, in lieu of using the Pandapower standard type library, we used information from a previously published JICA (2009) study on the energy system in the country. This study included estimated line property parameters based on line voltage capacities. These values were approximated and assigned to the lines in the modelled network based on the line capacities.

Using the network loading, topology, and properties information gathered thus far, the PyPSA package was used to run a power flow analysis that returned phase angles at every node. This was processed into casedata file ready to be input into the MATCASC model.

<sup>8</sup>Available at [energydata.info](http://energydata.info)

### 4.3 Flood risk in Sierra Leone

The Fathom-Global flood maps for Sierra Leone each comprise a 4000x4000 cell array making up a national grid of water depths given the specified flood event. Two exceedance probability curves (for fluvial and pluvial floods) were generated for each cell in the map (in this case, a total of 16,000,000 cells) using linear interpolation.

The USGS HydroSHEDS data set was used as a starting point to map the river basins in Sierra Leone, with reference to the river basin map developed by the [National Water Resources Management Agency Sierra Leone \(2015\)](#). A total of 12 river basins were delineated for Sierra Leone as shown in Figure 15. LHS was used to generate 200 flood scenarios by assigning flood events, as characterized by its exceedance probability, to each river basin and drawing the corresponding flood heights for all cells within.

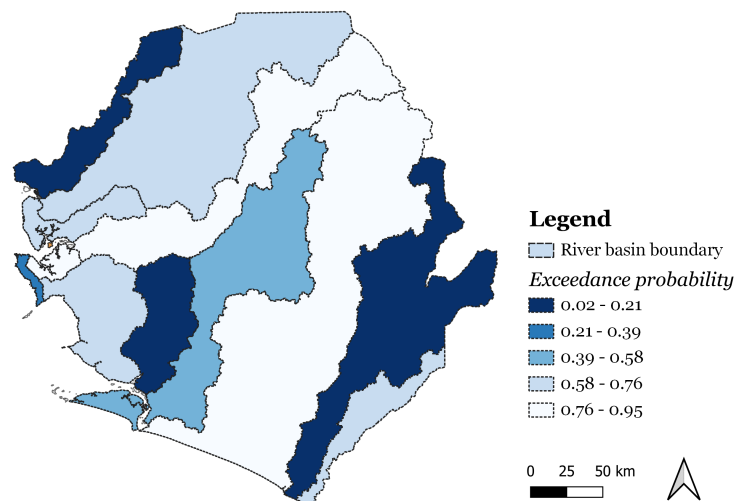


Figure 15: Visual representation of one flood scenario. Each river basin is assigned a flood event of a different intensity.

Using the grid cell fluvial and pluvial exceedance probability curves, flood heights can be drawn based on the flood event occurring in each river basin. The largest flood height of the two is then retained as the occurring flood height in the grid cell (Figure 6). This process is repeated for every cell on the grid in order to generate a flood map for the entire country.

The power network can then be overlaid with the generated flood maps, and flood heights at all of the nodes can be determined for each of the 200 flood scenarios. With the known flood heights, the probability of a node failing can be estimated based on fragility curves (Figure 8) as described in Chapter 3. By sampling the probability of failure of the node 1000 times per flood scenario and identifying the overall rate at which the node fails, we estimate the level of flood risk of the nodes. The lines that are directly connected to these nodes are then identified as initial line threats which are input into the MATCASC model alongside the casedata generated in Chapter 4. For these simulations, we assume a conservative tolerance parameter ( $\alpha$ ) of 1 for the transmission lines, indicating that there is no excess capacity in the lines.

#### 4.4 Quantifying impacts

With the casedata inputs for the power network and the initial failed line known, the cascading failures can be simulated with MATCASC. The model outputs were processed such that the specific cluster locations that experience a power outage can be identified. We were thus able to estimate the size of the population impacted (i.e., those residing in the impacted cluster locations). The MATCASC model also included a module that enabled quantification of the total power lost (or demand not met).

To explore alternative metrics for characterizing the impacts of these failures, we investigated the DHS Program data set for Sierra Leone. This data set comprises responses from a total of 69,871 individuals across 557 survey clusters tagged with GPS coordinates (Stats SL & ICF, 2020). Using Empirical Bayesian Kriging, two maps of Sierra Leone were generated: one showing the proportions of poor households, and another showing the proportion of women-headed households (Figure 16). These indicators are selected in accordance with the literature reviewed and summarized in 2.3.

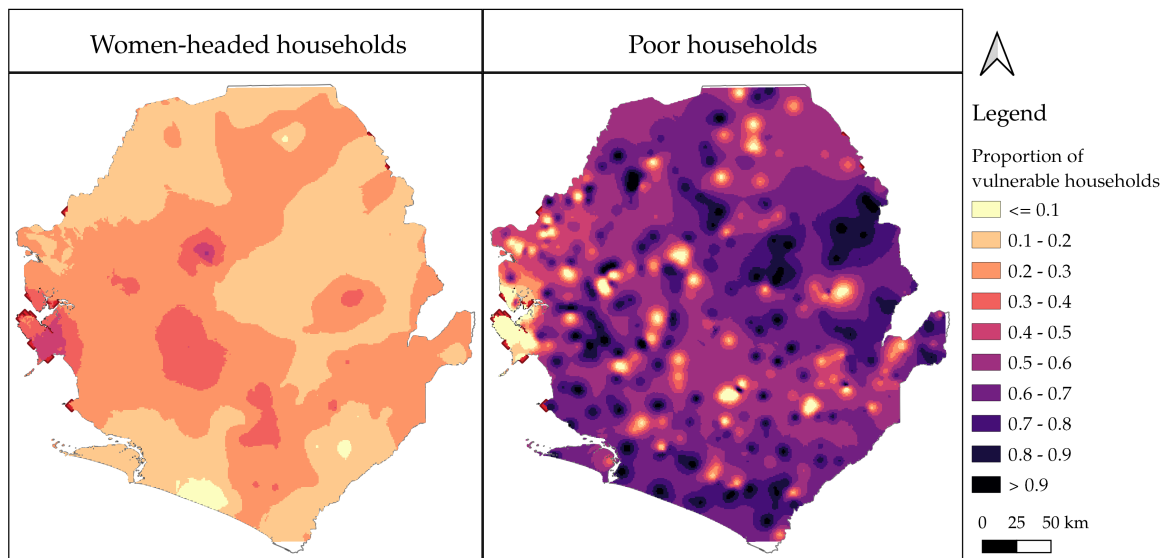


Figure 16: Maps indicating proportion of vulnerable households, based on interpolated statistics.

Overlaying the cluster locations with the interpolated maps allows estimation of the proportion of women-headed households and poor households per cluster location. With the known population counts in each cluster, the size of the population belonging to women-headed or poor households can be approximated. Once it is known which cluster locations suffer power outages, the characteristics of the impacted population can be calculated and the relative impacts of an outage on vulnerable population groups may be assessed.

## 4.5 Policy evaluation

The example policy interventions added parallel links along the high-voltage transmission line from Bumbuna to Freetown (three examples are shown in Figure 17). This is implemented by identifying all pairwise combinations of nodes along the high-voltage (161 kV) transmission line from Bumbuna to Freetown, and adding a link in between each of those pairs of nodes. This resulted in 120 unique modifications to the network. Network performance is evaluated for each policy under all damage state scenarios.

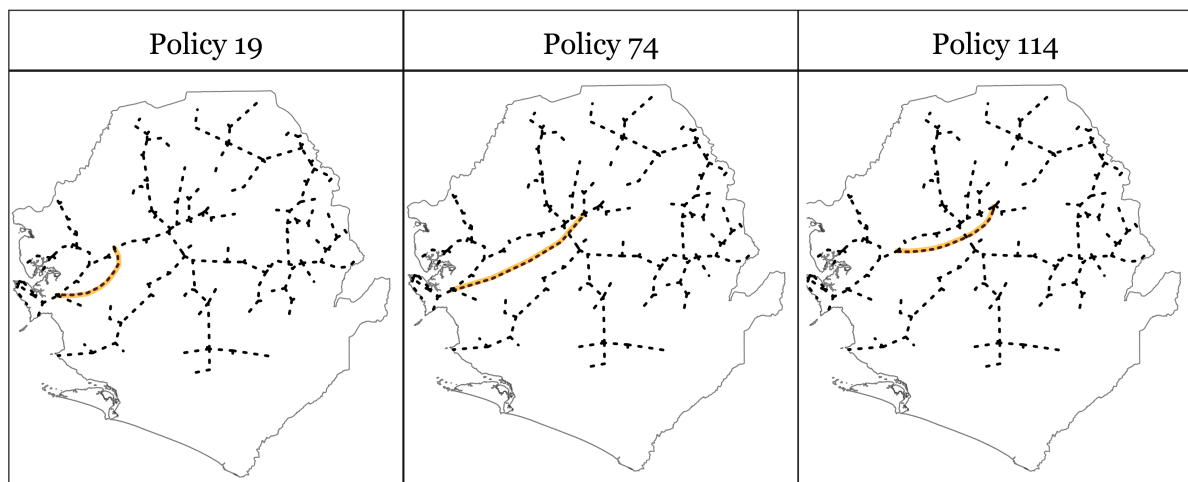


Figure 17: Graphical representation of 3 of 120 iterations of link additions (highlighted in yellow) to the network.

The policy interventions are evaluated in terms of impacts on total demand lost, poor households impacted, women-headed households impacted, as well as implementation cost. In this study, the length of each link is used as a proxy for the cost of implementing the intervention. This assumes that the longer the new transmission line, the higher the implementation cost. This enables a comparison of relative costs associated with each new line added to the network.

A complete list of the evaluated policy interventions is shown in Appendix [A.1](#).

## 4.6 Climate change impacts

We obtained the RCP4.5 scenario maps for projected average maximum 1-day precipitation and generated maps indicating rates of change for the available time periods for Sierra Leone. Based on these rates of change, we modified the exceedance probability curves used for deriving the flood maps and, for each future time period, created 200 new flood maps based on the 200 river basin flood scenarios. Figure 18 shows an example of one flood scenario for the base case and the future time periods.

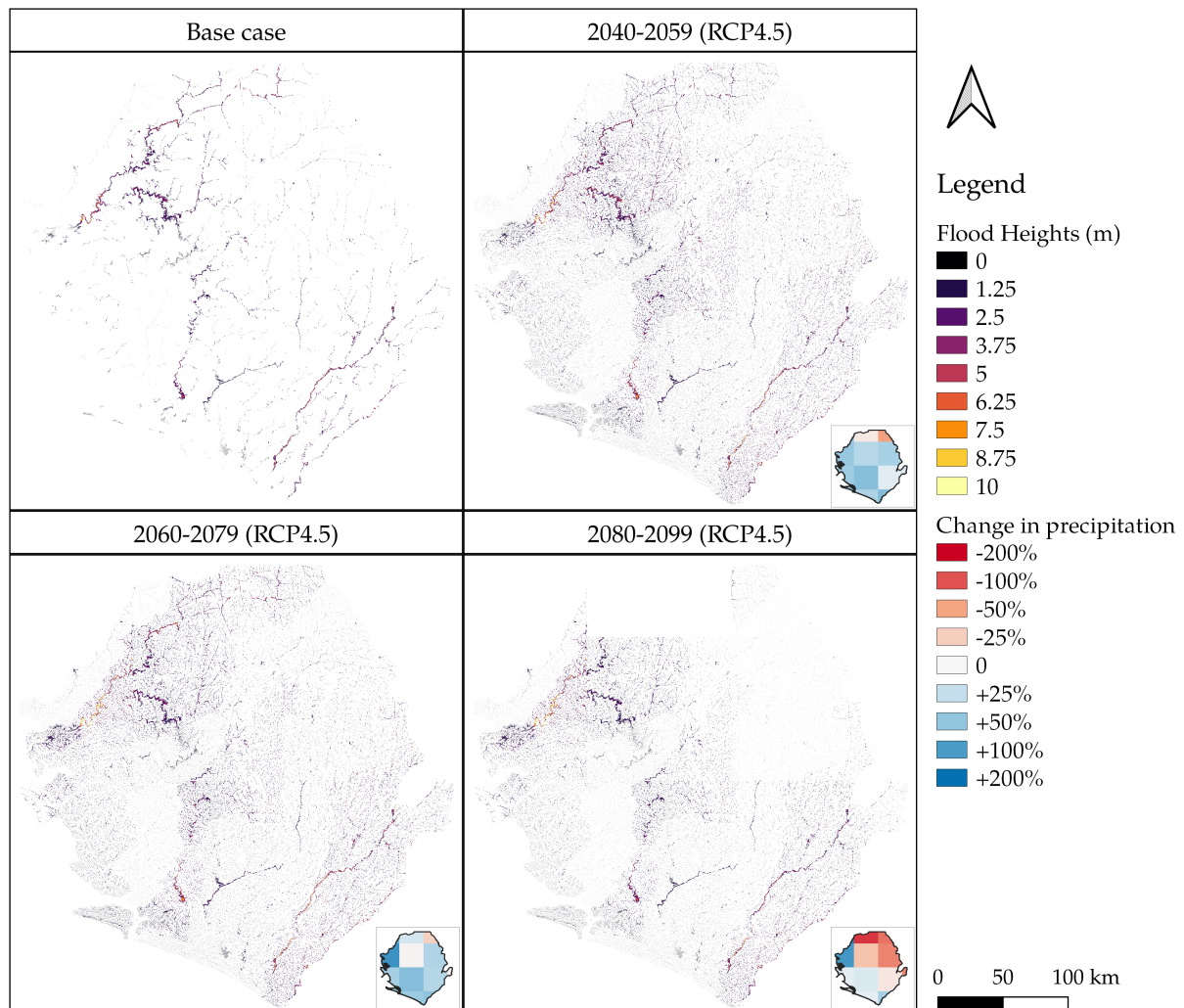


Figure 18: Flood maps for one example scenario, modified to account for projected climate change impacts. Inset maps show projected change in maximum 1-day precipitation.

For some areas in Sierra Leone (i.e., grid cells shown in shades of red on the inset maps in Figure 18), the projections indicated a decreasing trend in the maximum 1-day precipitation values for future time periods. These areas are identifiable in the resultant flood maps where the flood depths are shown to be lower.

## 4.7 Validation and sensitivity analysis

It is necessary to validate the methods for deriving the data inputs described in this chapter using verifiable sources of information. Two primary sources of data were used: global satellite imagery and national census data.

Firstly, Visible Infrared Imaging Radiometer Suite-Day Night Band (VIIRS-DNB) nightlights imagery was processed for Sierra Leone and compared alongside the derived power transmission network. It is assumed that the areas along the derived power transmission network should be approximately aligned with areas indicated as lit in the nightlights images.

The Sierra Leone National Census was most recently conducted in 2015 and contains survey responses from individuals that are tagged with high-resolution enumeration areas (Figure 19).



Figure 19: Enumeration areas in the 2015 Sierra Leone national census.

To validate our approach, we compared 2015 census enumeration area statistics with the total and vulnerable population count estimated using WorldPop and the DHS Survey interpolation method. The discrepancies are shown in the following chapter.

Finally, we conducted a sensitivity analysis to determine if some of the assumptions might significantly impact the model outputs. This is intended to identify the variables and assumptions which might contribute to inaccuracies in model outputs. The variables tested include:

1. **Distribution of loads**, to review changes in network performance resulting from small changes in load distribution. Specifically, this is to evaluate the effect of assuming that the distribution of load is directly proportional to the distribution of population.
2. **Reactance of transmission line**, to review changes in network performance resulting from small changes in assumed transmission line reactance.
3. **Capacitance of transmission line**, to review changes in network performance resulting from small changes in assumed transmission line capacitance.

We varied each of the above variables incrementally and regenerated MATCASC inputs, and subsequently re-simulated the cascading failures. We calculated the total power lost for each variation and plotted these results alongside base case outputs.

## 5 Results

This chapter first presents the nodes (substations in the power network) that are exposed to flood risk and the consequent damage states that emerge. Subsequently, results from the cascading failures and impacts analysis are shown. Additionally, we show the outcomes of the policy interventions and evaluate the performance of the policies. The flood risk analysis that accounts for future climate change impacts is presented next, and the chapter concludes with validation and sensitivity analysis outputs.

### 5.1 Flood risk analysis

As described in Chapter 4, 200 flood scenarios were generated. Given the flood depths at each node and the corresponding probability of failure, we sampled the probability of failure 1000 times per flood scenario in order to estimate the levels of flood risk that the nodes are exposed to. The outcomes of this exercise are a set of failed nodes (or node) per flood scenario, and the number of times the node fails. It was found that there are nine possible damage states, which consist of four nodes exposed to flood risk, and five combinations in which two or more of the four nodes fail simultaneously.

Figure 20 shows the four individual nodes exposed to flood risk and their rates of failure (calculated as the number of times the node fails over the 1000 failure simulations \* 200 scenarios) and degrees centrality. This aggregate failure rate is used as a proxy for the level of (flood) risk that the nodes are exposed to. The node degree centrality indicates the number of links directly connected to that node and is a purely topological metric used to highlight the importance of a node in a network.

It was found that while node 125 has a degree centrality of only 1, it experiences the highest flood risk (i.e., the highest failure rate). Meanwhile, node 66 has a relatively higher degree centrality, but a relatively low flood risk. The results also show that node 33 faces the lowest flood risk, with a node centrality of 1 and a failure rate of 0.000045. Figure 21 shows the location of these nodes within the power network.

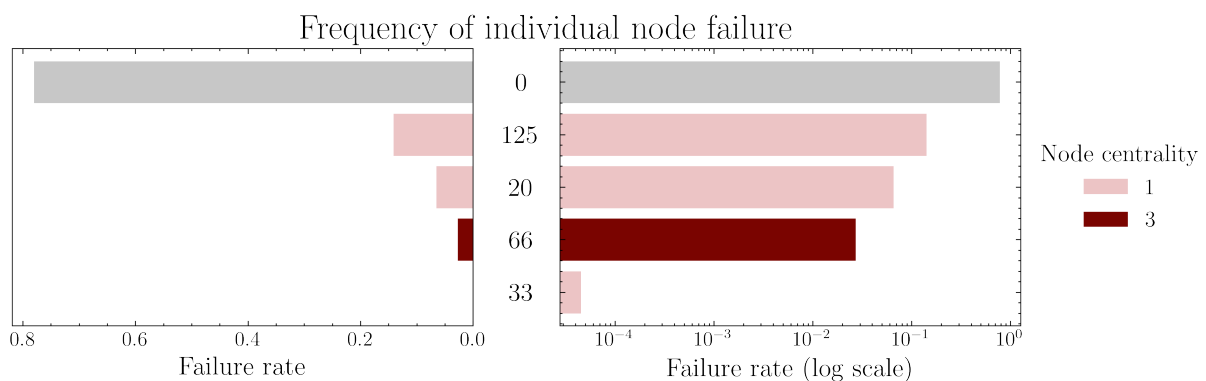


Figure 20: Nodes with high flood risk, node degree centrality and aggregate failure rate shown in regular scale and log scale.

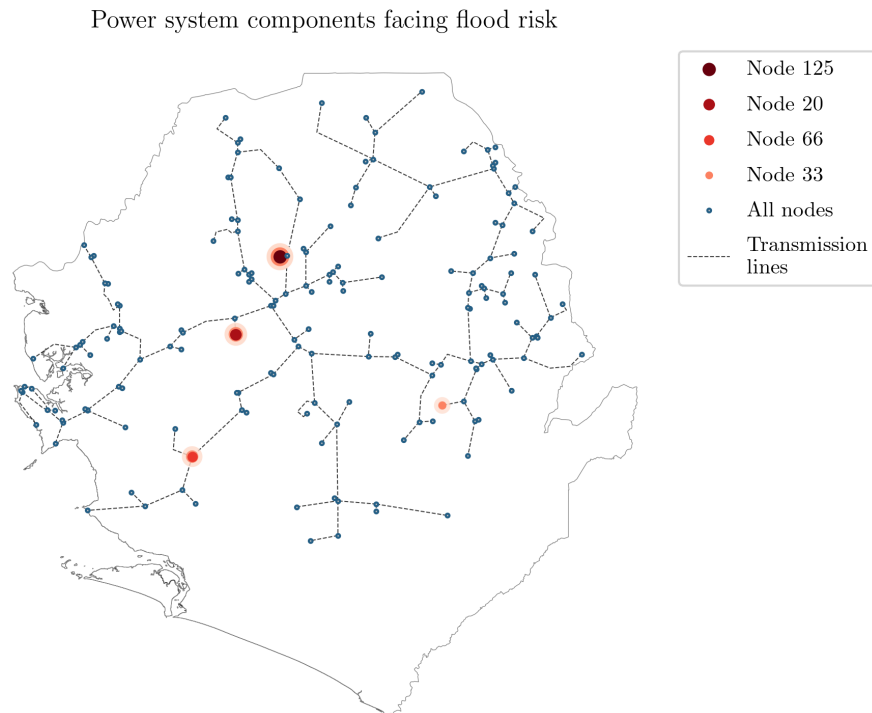


Figure 21: View of nodes in the power network with risk of failure due to floods. Darker and larger nodes represent higher risk.

Figure 22 shows the nine damage states and their rates of failure. The failure rate for the damage states provides an indication of the likelihood of each damage state scenario occurring and allows for a ranking of the damage states in terms of the level of risk.

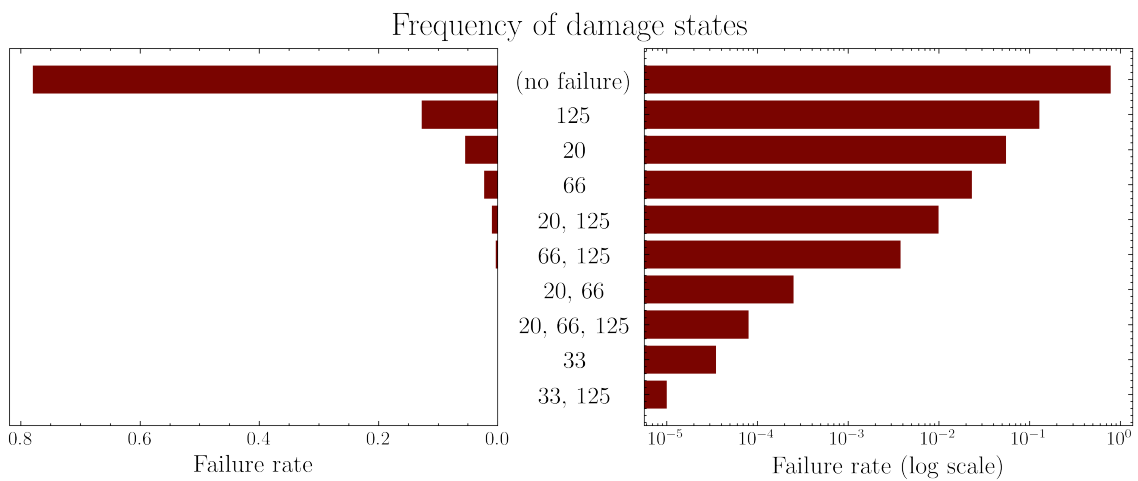


Figure 22: Failure rates of all damage states that may occur, shown in regular scale and log scale

## 5.2 Cascading failures analysis

The damage states were converted into MATCASC inputs to investigate how the cascading failures triggered by those initial node failures propagate through the network. Figure 23 shows plots of the geographic extents of the cascade for two damage states. It can thus be seen how the failure spreads through the network and affects other areas not exposed to flood risk. Appendix A.2 contains maps for the remaining damage state scenarios.

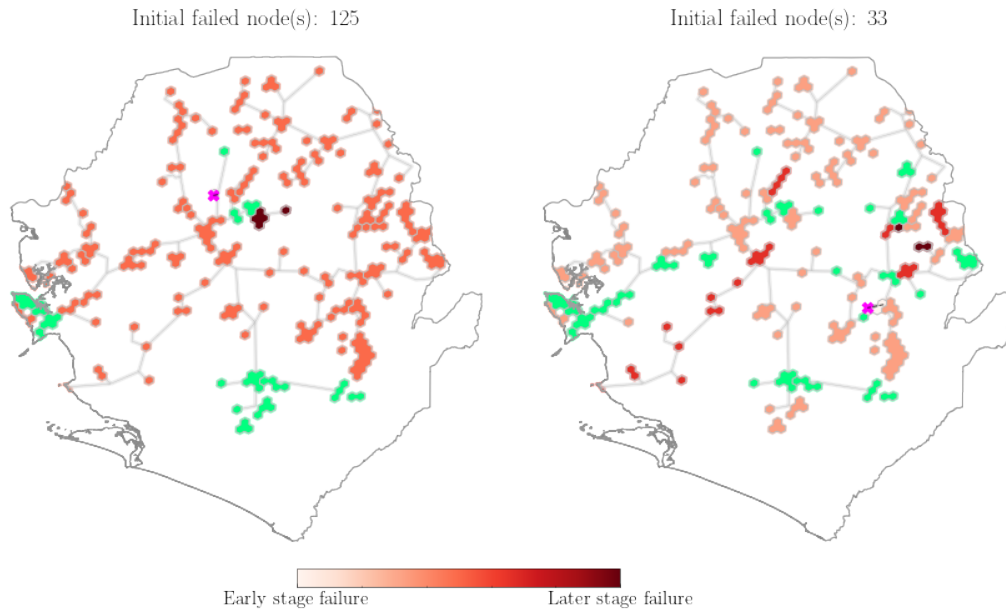


Figure 23: Visual representation of the cascading failure that occurs with the failure of individual nodes 125 and 33. The cluster locations that experience the initial outage are colored in light pink, while the cluster locations that experience an outage in later stages of the cascade are colored in darker shades of red. Areas that do not suffer a power outage are shown in green.

Furthermore, these figures indicate the stage in the cascade at which cluster locations experience an outage. As MATCASC iteratively redistributes power loads and removes all overloaded lines accordingly, model users may identify nodes that fail in the earlier stages, and which thereby triggering additional later stage failures.

The estimated impacts resulting from each of the damage states are quantified and shown in Table 1 and Figure 24. The results show that the most severe damage state scenario in terms of size of the power outage is when nodes 20/66 fail in tandem, leading to a 99% reduction in service delivery and the highest number of people affected. In contrast, the failure of individual node 20 leads to the least total power loss.

Table 1 further enumerates the percentage of the population impacted by power outages that are from poor or women-headed households, thereby demonstrating that some damage states cause a disproportionate impact on some population groups over others. The results show that some damage states will impact a higher number of poor households (e.g., node 66), as compared to the damage state scenarios where nodes 20/66 and nodes 20/66/125 fail in tandem.

Damage states	Proportion of total power lost	Population losing power	Proportion of Women-headed HH losing power	Proportion of Poor HH losing power
20	0.337	1101762	0.282	0.333
33	0.337	1103685	0.281	0.331
125	0.36	1186195	0.28	0.334
33, 125	0.502	1690938	0.288	0.309
66	0.596	2027497	0.295	0.283
66, 125	0.601	2044896	0.296	0.284
20, 125	0.603	2054712	0.295	0.287
20, 66, 125	0.891	3082212	0.305	0.173
20, 66	0.991	3442097	0.308	0.173

Table 1: Impacts for each damage state scenario in the base case.

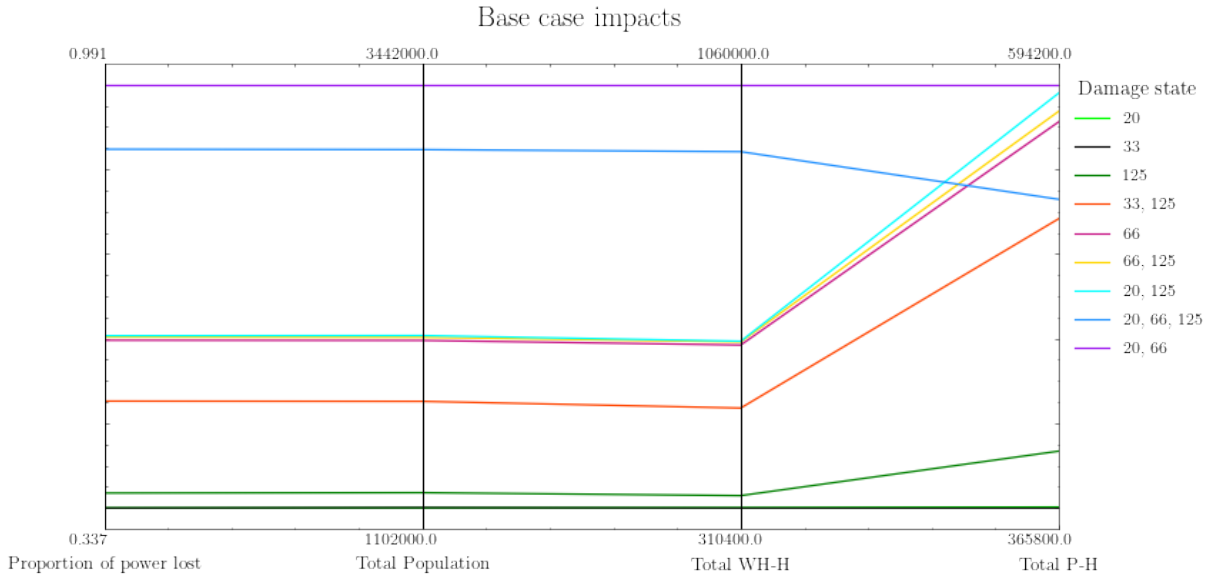


Figure 24: Parallel plot showing comparison of impacts between damage states. The metrics are shown on each of the axes.

### 5.3 Policy Considerations

The policies shown in Chapter 4 were analysed in MATCASC for all 9 damage state scenarios, and policy performance was calculated by assessing the impacts of the resultant failures, post-policy implementation, in terms of four metrics: (i) cost of implementation, (ii) size of population impacted, (iii) proportion of population from women-headed households impacted, and (iv) proportion of population from poor households impacted.

The average performance of the policies across all damage states was determined and ranked based on each of the four metrics (Table 2). Decision-makers have various criteria for policy selection and may favor either of these policies depending on their policy objectives. For example, a decision-maker whose objective is to minimize intervention costs may favor the implementation of Policies 14 over the other policy options. For a holistic assessment of intervention efficacy, the set of policies should be evaluated against each other and in terms of trade-offs between

performance metrics.

Metric	Objective	Policy
Population losing power	Minimize	Policy 70 and 19
Women-headed households losing power	Minimize	Policy 71 and 19
Poor households losing power	Minimize	Policy 19 and 114
Cost (length of added link)	Minimize	Policy 14

Table 2: Set of policies that yield best performance per metric.

The relative performance of the set of policies across the trade-offs and against each other can be displayed in a parallel coordinates plot as shown in Figure 25, which shows outcomes for the most severe damage state in terms of total power lost (simultaneous failure of nodes 20 and 66), and Figure 26, which shows outcomes for the most likely damage state (failure of node 125). Parallel coordinates plots can be a useful visual aid for further filtering down a set of policies for more careful consideration.

For example, Figure 25 shows that, for this damage state scenario, Policy 114 will outperform all the other policies in terms of the three metrics for population impacted (total, women-headed households, and poor households). When cost is taken into consideration, both Policies 19 and 114 outperform the other policies in all four metrics. Given this, a decision-maker may decide to remove the other policies from consideration and focus more closely on evaluating those two policies only.

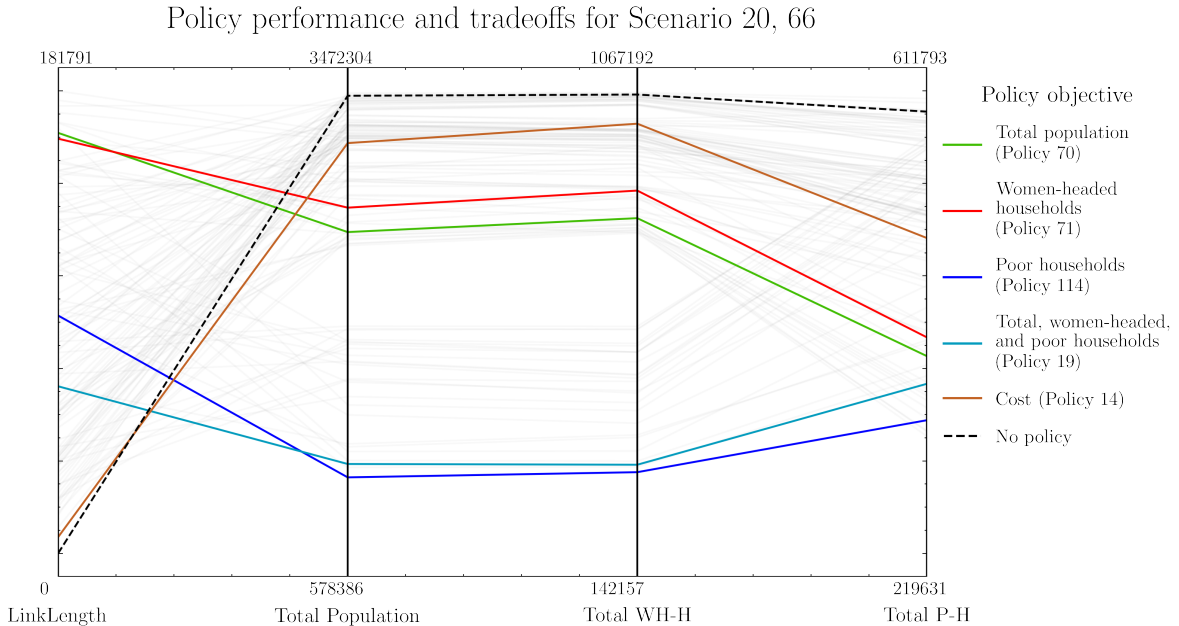


Figure 25: Parallel plot showing tradeoffs between a set of policies that minimize each of the metrics, represented by the vertical axes.

For the most likely damage state, Figure 26 shows that the set of selected policies yield worse outcomes for all metrics across the board as compared to the base case (No policy) outcomes. In this situation, it appears that increasing network redundancy by adding parallel lines to the high-voltage line in the network is a poor strategy. This phenomenon is consistent with Braess's Paradox, which is the observation that adding one or more links to a network can

worsen overall network performance (Blumsack, 2006; Witthaut & Timme, 2012). Decision-makers may do well to pursue other options to strengthen the flood resistance of node 125, such as by raising sensitive equipment to a higher elevation.

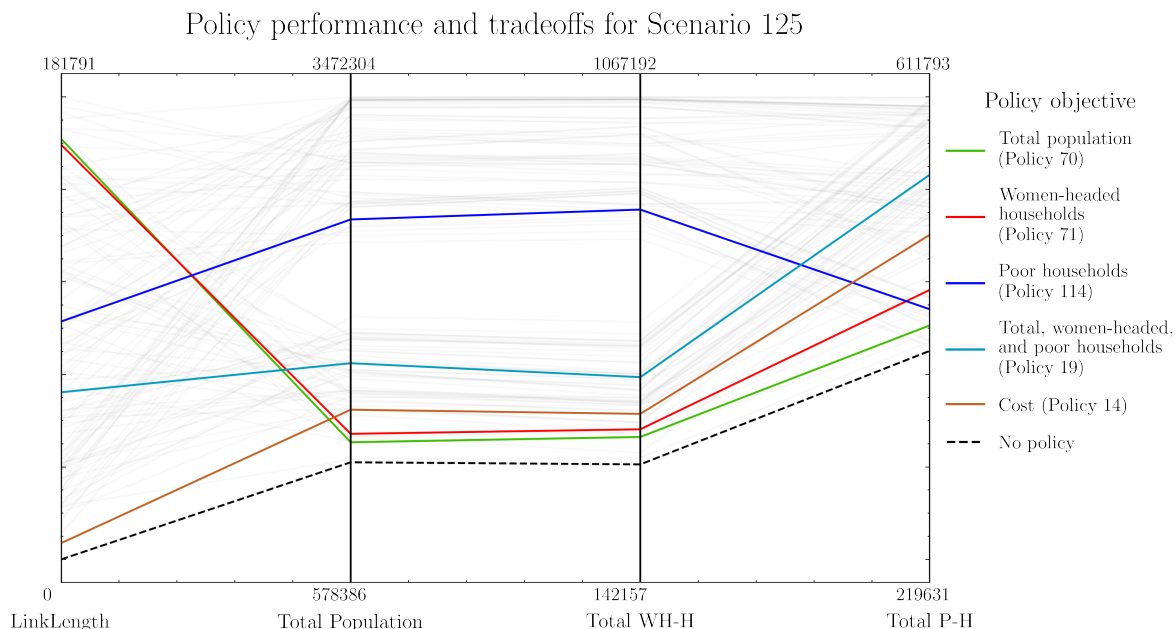


Figure 26: Parallel plot showing tradeoffs between a set of policies that minimize each of the metrics, represented by the vertical axes.

## 5.4 Climate change impacts

To take into account considerations for potential climate change, we modified the exceedance probability curves of the flood events and generated new flood maps based on future projections for extreme rainfall. The new flood maps revealed an additional set of 5 nodes (on top of that found in the base case) that experience flood risk. The varying levels of flood risk of each node is shown in Figure 27. The locations of the individual nodes are shown in Figure 28.

Figure 27 indicates that, while the flood risk of individual nodes varies, there is a general decreasing trend of flood risk given the projections for average maximum 1-day rainfall. The same results are shown in Figure 29, clearly indicating a reduction in flood risk of the exposed nodes in each successive future time period.

The analysis also indicates that the 9 individual nodes may fail in a total of 73 different combinations. The flood risk of the top ten most likely damage states is shown in Figure 30.

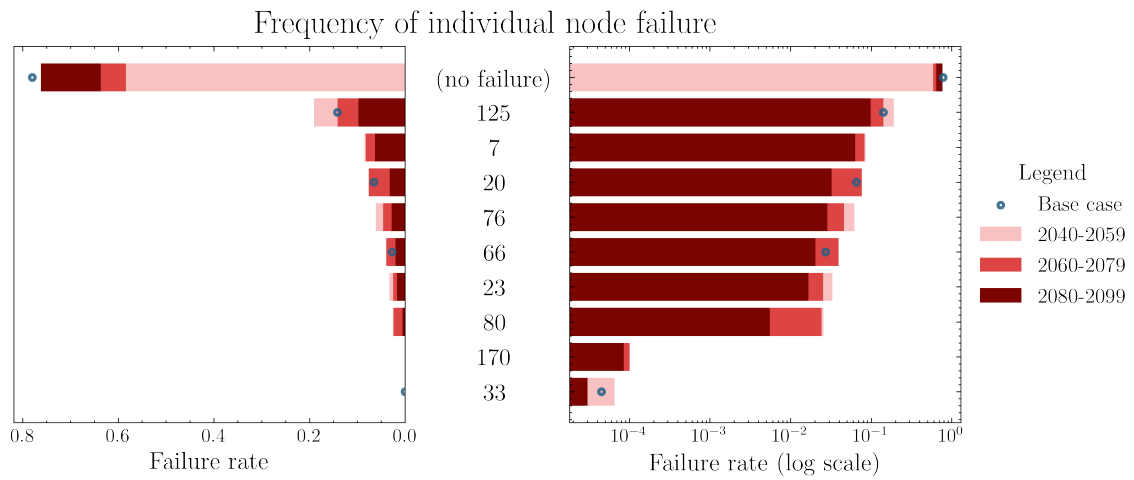


Figure 27: Failure rate of nodes with flood risk under future climate scenarios, shown in regular scale and log scale.

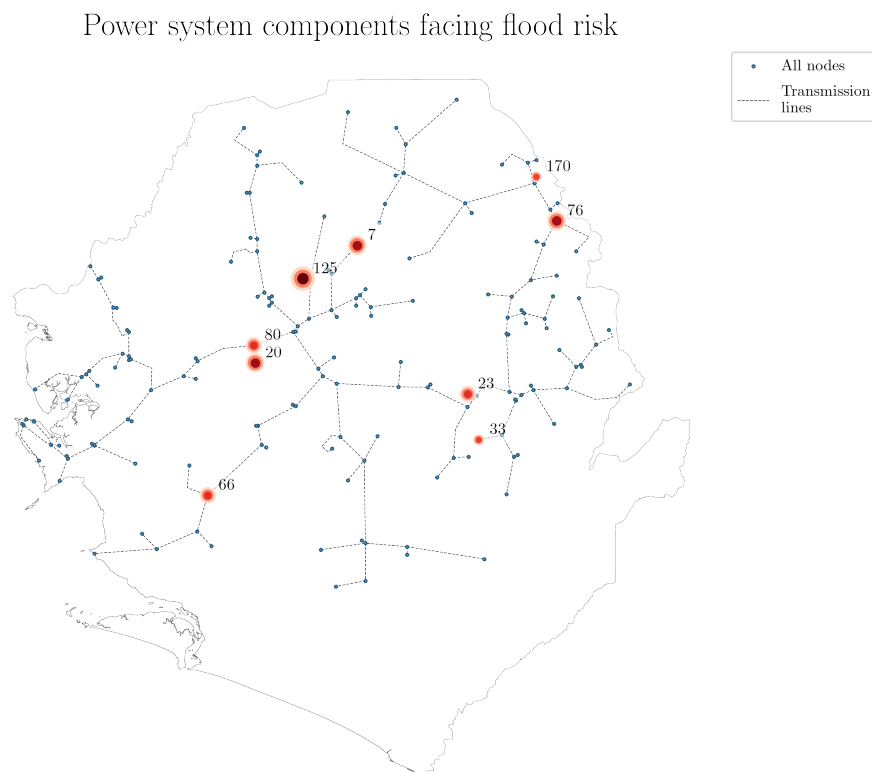


Figure 28: View of nodes experiencing flood risk under future climate scenarios. Darker and larger nodes represent higher risk.

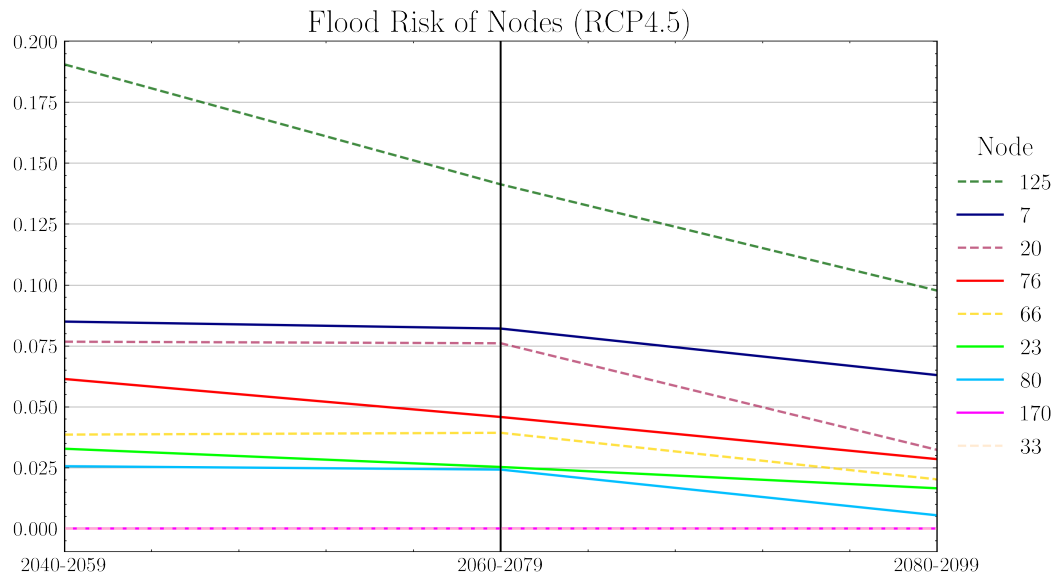


Figure 29: Parallel plot indicating estimated change in failure rates of exposed nodes in future time periods under RCP4.5.

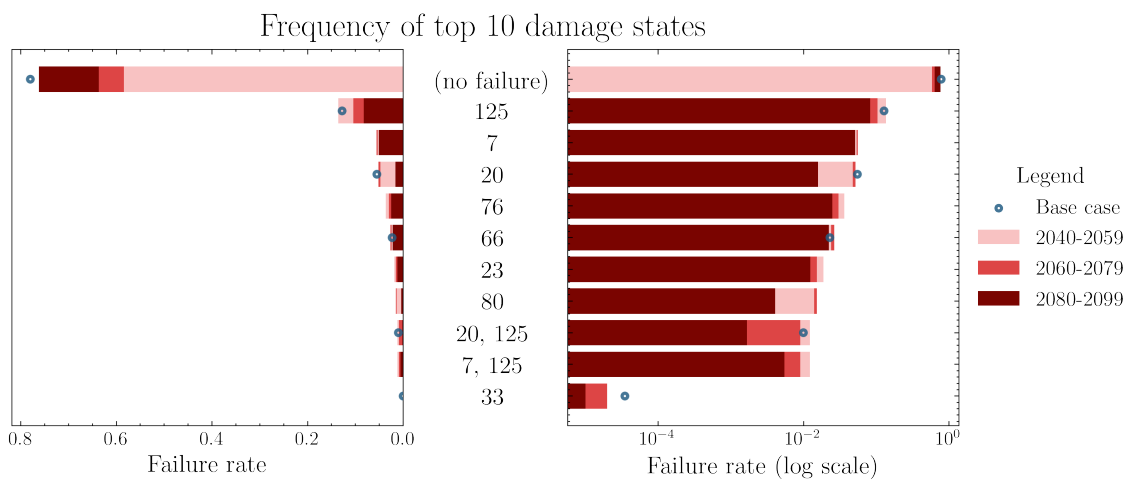


Figure 30: Failure rates of the top 10 most likely damage states under future climate scenarios, shown in regular scale and log. scale. Dashed lines indicate nodes that experience flood risk in the base case.

## 5.5 Validation and sensitivity analysis

The monthly composite images of the VIIRS-DNB nightlights data set were collected, overlaid with the derived power network, and visualized (two example images are shown in Figure 31). The objective was to visually confirm whether the distribution of nightlights intensity is consistent with the derived power network lines. It was found that the nightlights are approximately spread out in close proximity of the power network lines and that these lights appear to be expanding around network lines over time.

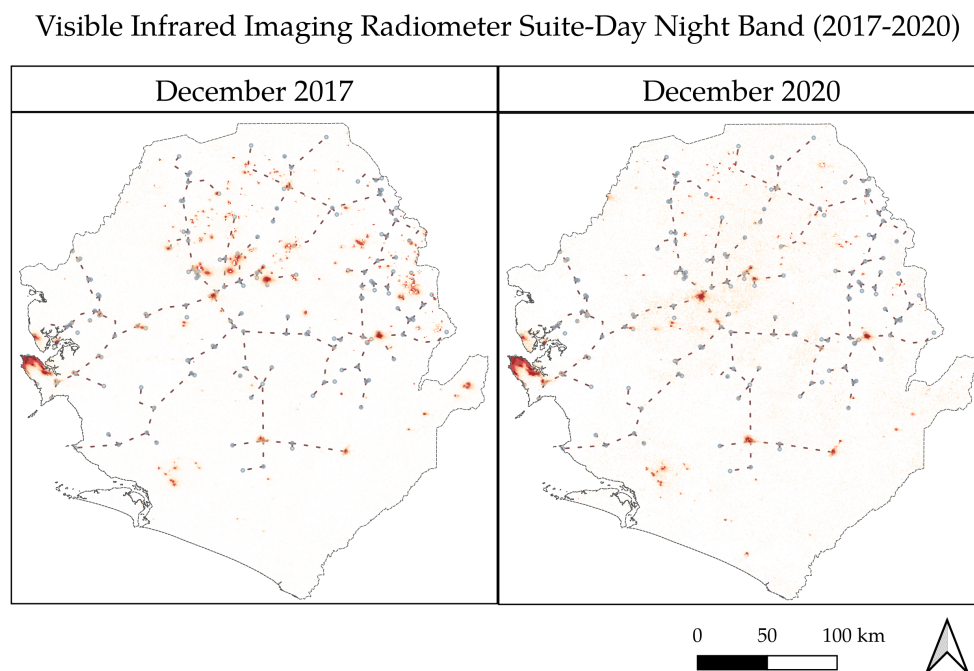


Figure 31: Overlay of December 2017 and 2020 VIIRS-DNB nightlights images in Sierra Leone with the derived power network data.

To validate the WorldPop population counts data set, we used the population breakdown by chiefdom obtained from the 2015 national census and compared it with the WorldPop population estimates for each chiefdom. It was found that the WorldPop data set overestimates population counts for chiefdoms in the southern areas of the country (e.g., in Bo and Kenema Districts), and that the overestimation occurs on a larger magnitude (up to 130 %) than the underestimation (up to 65%). It was also found that WorldPop overestimates the population in Freetown by approximately 120%.

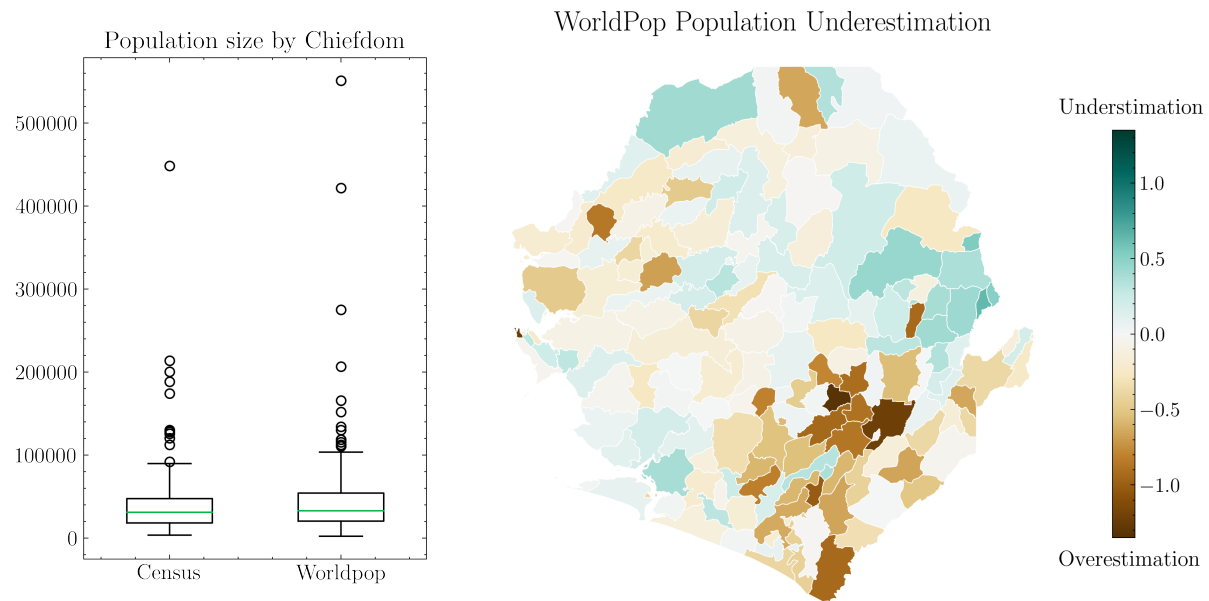


Figure 32: Boxplot (left) shows distribution of Chiefdom population sizes as indicated in the 2015 national census and WorldPop estimates. WorldPop discrepancies (over- and under-estimations) as compared to the census data are spatially plotted in the choropleth (right).

Plots characterizing the distribution of discrepancies across the chiefdoms may be found in Appendix A.3.

We compared the proportion of poor households in each enumeration area in the 2015 national census with estimates for the same indicator obtained by interpolating cluster statistics from DHS survey data. The boxplot in Figure 33 indicates that the DHS method underestimates the proportion of poor households in many areas.

Furthermore, we intersected the cluster locations with the enumeration areas to obtain the mean indicator values for the cluster locations. Where a cluster intersects with more than one enumeration area, the average of the statistic for all overlapping enumeration areas is used. The discrepancies are plotted in the choropleth shown in Figure 33. It was found that the underestimation occurs on a larger magnitude (up to 100 %) than the underestimation (up to 20%). The proportion of poor households are underestimated most notably (up to 99%) in the Western Areas and in Port Loko.

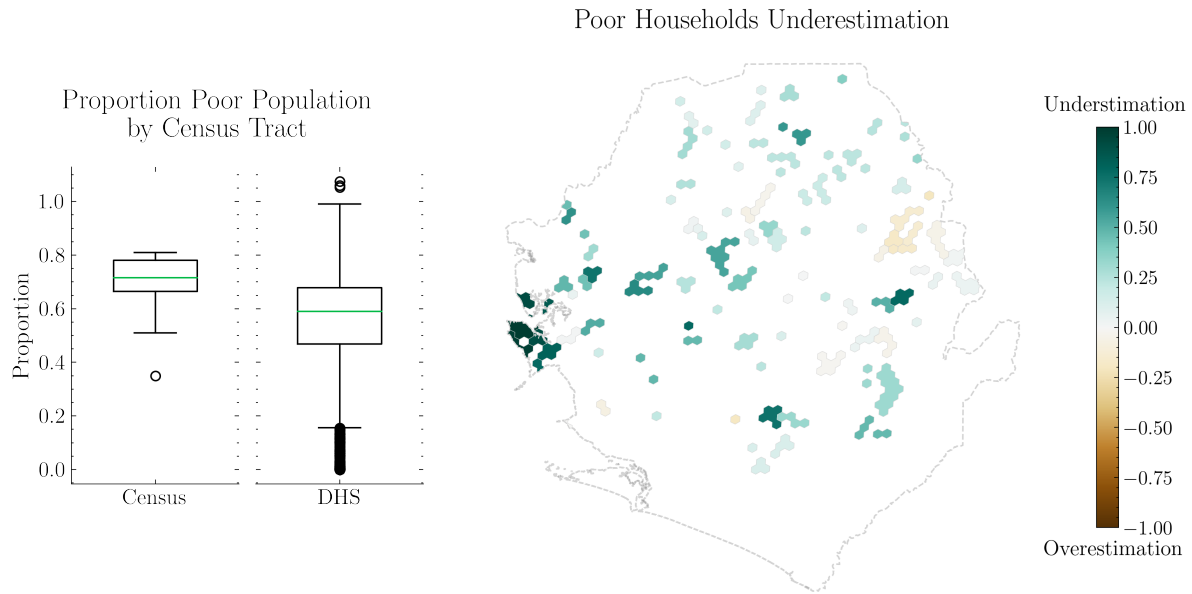


Figure 33: Boxplot (left) shows distribution of estimated proportion of poor households as indicated in the 2015 national census and DHS survey estimates. Discrepancies between the DHS survey estimates and the census data are spatially plotted in the choropleth (right).

We used the same method to validate the proportion of women-headed households in Sierra Leone as estimated using DHS survey data. Using both the national census data and interpolated DHS survey maps, we determined the proportion of women-headed households for all enumeration areas and compared both values. Figure 34 shows that, in aggregate, the DHS method underestimates the proportion of women-headed households, albeit the magnitude of the underestimation appears to be smaller than that for poor households. We also reviewed the discrepancies in the estimates for the cluster locations, which is shown in the choropleth in Figure 34. The choropleth indicates that the magnitude of overestimation of women-headed households is the largest in the York Rural chiefdom (in the Western Area Rural district), by approximately 95%, while the largest underestimation occurs in the Koinadugu district at approximately 62%.

Plots characterizing the distribution of discrepancies in the DHS indicators across the cluster locations may be found in Appendix A.3.

The sensitivity analysis results showed the model outputs are not sensitive to changes in transmission line properties such as capacitance and apparent power limits. However, we found that model outputs are sensitive to changes in the initial distribution of loads, with the range of outputs varying from 3% to 26% based on the damage state scenario. Furthermore, we found that variations in the transmission line reactance alter model outputs for service reduction, with the range of outputs varying from 20% to 42% based on the damage state scenario. The results of the sensitivity analysis are plotted and shown in Appendix A.4.

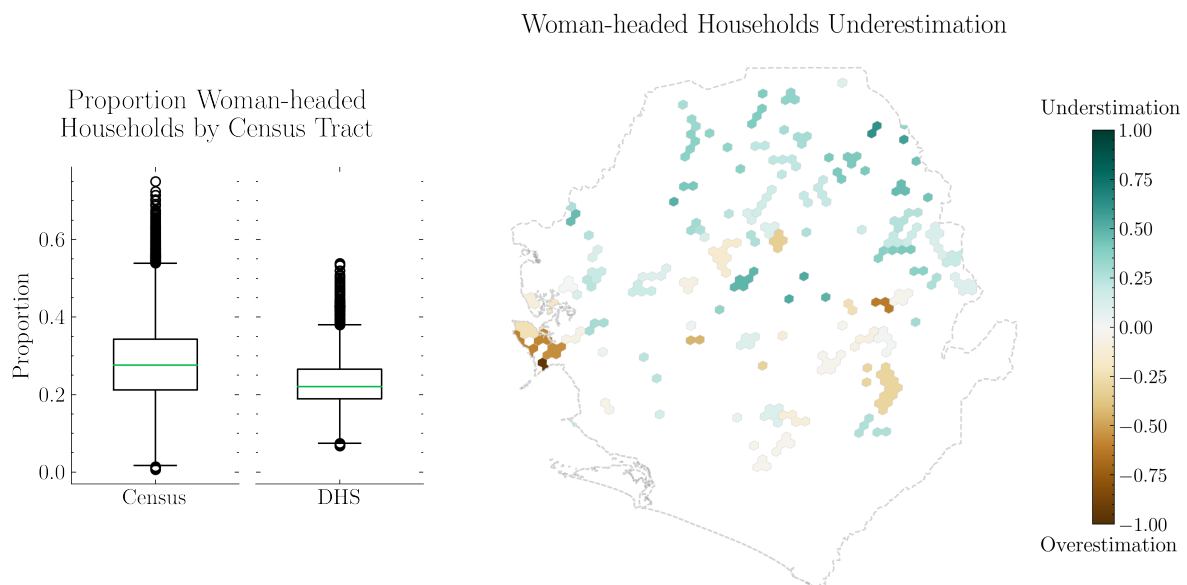


Figure 34: Boxplot (left) shows distribution of estimated proportion of women-headed households as indicated in the 2015 national census and DHS survey estimates. Discrepancies between the DHS survey estimates and the census data are spatially plotted in the choropleth (right).

## 6 Discussion

This chapter discusses the findings yielded by the proposed method and the results for the case study application shown in Chapter 5. We also present a discussion on the validation of the input data.

### 6.1 Findings

The proposed method for answering the research question is composed of a flood risk analysis, a cascading failures analysis, and an impacts analysis. The flood risk analysis enables a policy maker to identify components of a power network that are exposed to flood risk (e.g., the four network nodes shown in Figure 21), thereby providing focal points for policies or projects aimed at reducing the flood risk of a power network. The method also reveals the level of risk (failure rates) associated with each failed node.

In the case study, it was found that node 66 had the highest degree centrality (Figure 20). When considering individual node failure, the failure of node 66 ultimately resulted in the largest service reduction, as compared to all other damage state scenarios in which only one node failed (Table 1). Although node 66 has a smaller level of risk than node 125, it constitutes a potentially impactful target for improvements to the network.

Knowing the full set of damage states and their likelihoods further enriches the planning process for network improvements. For example, in knowing that damage states involving node 33 are substantially less likely than all other damage states, policy makers may wish to focus initial investments on nodes 125, 20, or 66 only (Figure 22).

The cascading failures analysis shows how an initial failure propagates through the network and causes power outages in far-off areas of the country (Figure 23). Nodes that fail in the early stages play a role in exacerbating the cascade of failures. Policy makers may therefore wish to focus on strengthening or building redundancy into those nodes so as to limit the propagation of a cascading failure.

The impact analysis provides policy makers with two perspectives with which to approach the policy-making space for reducing disaster risk in power networks:

1. Technical perspective, whereby impacts are assessed in terms of total power loss, and
2. Welfare perspective, whereby the total populations impacted as well as their characteristics are taken into account. In this research, we consider the proportion of the impacted population from poor households and women-headed households.

The impacts of the cascading failures can be measured in terms of these metrics, therefore providing multiple ways to frame the impacts of the various damage states and the cascading failures. It should be noted that other metrics may be selected in accordance with the policy objectives.

For all damage state scenarios considered in our case study, we found that the proportion of the population from women-headed households is not disproportionately impacted when com-

pared with the general population. This is likely because the spatial patterns of distribution of women-headed households and the general population are similar (i.e., the larger the population in an area, the more women-headed households).

However, a disproportionate impact can be seen in the case of poor households. Table 1 showed that:

1. Poor households make up a relatively high proportion of the population impacted when higher frequency and lower magnitude failures occur.
2. In the case of lower frequency and higher magnitude failures (for example, 89% and 99% power loss), the proportion of poor households impacted is smaller.

The combination of these three analyses allows a policymaker to identify focal points for assessment of network performance in accordance with their policy objective.

We demonstrate how this method may be used to assess policy interventions that entail expanding the power network. The resultant change in network performance under those interventions can then be compared to the base case network performance. We demonstrate that the impact analysis provides a systematic way to evaluate and compare multiple potential policy options against each other, and informs the process of ranking and filtering out policy options that perform worse on all metrics (Figures 26 and 25). This method can also be used to test other intervention strategies in the network, such as adding generators or testing alternative loading conditions.

We further demonstrate how the method may be adapted to explore the impacts of uncertain future scenarios. We considered the potential impact of climate change by quantifying the rate of change in extreme rainfall across space and time and generated new flood maps based on those changes. Given the assumption that flood occurrence is correlated to extreme rainfall, the analysis shows that even though more power network components are exposed (Figure 28), the levels of flood risk of those components reduce over time (Figure 30). This should be considered alongside other contextual factors as the reduction in flood risk (as linked to reducing precipitation) may adversely impact the power network in other ways. For example, reduced precipitation may lead to drought occurrence, which can worsen disruptions to the power supply as hydroelectric power forms a large part of the Sierra Leone energy generation portfolio.

While this example demonstrated consideration of future climate change scenarios, policy makers may adapt the method to understand the potential impacts of other external factors as well. For example, policy makers can explore how increased urbanization impacts the severity of cascading failures and the resultant stability of the network by increasing the concentration of load consumption in urban centers.

## 6.2 Validation and sensitivity analysis

The goal of the validation exercise was to validate the method of deriving information from global data sets with alternative and verifiable data sources. Oftentimes, such data sources are unavailable or may not exist. Figure 31 demonstrates a surface-level approach to using satellite imagery to validate the derived data. Given that intensity of night-time lights is often a proxy

for electricity access (Doll & Pachauri, 2010), we visually assess whether high radiance levels (night-time lights), as detected by satellites, are centered around the derived power network. Evaluation of 2014 to 2020 monthly composite images for night-time lights from VIIRS-DNB indicated that there are consistent and visibly high radiance levels in the vicinity of the derived transmission lines, indicating the presence of power supply in those areas.

We used monthly composite images as downloaded from Google Earth Engine for this validation exercise. However, this method may be strengthened with the use of daily satellite images for night-time lights. The change in radiance levels from one day to the next can be quantified and mapped for the days before and after historical power outage events. It would be expected that areas with clear reductions in radiance levels after such events are indicative of the presence of a power network.

The comparison of population statistics derived from the DHS survey and WorldPop with the 2015 national census data shows that there is a wide range of overestimations and underestimations for the indicators considered. While estimates for at least half of the 91 clusters of the case study fall within a discrepancy range of 25% for both poor and women-headed households, there are wider discrepancies (over 90%) in urban areas where larger populations reside. These inconsistencies may introduce substantial inaccuracies in the estimated impacts when considering absolute numbers (e.g., size of the population impacted who are from poor households).

Some discrepancies in the information estimates may be due to the different collection times of the data sets. While the WorldPop data set contained projections for population counts in 2020 and the DHS surveys were conducted in 2018, the census surveys were conducted in 2015. It is plausible that the discrepancies shown in Figures 32, 33, and 34 indicate patterns of change in population statistics that occurred in between those years. One way to deal with the discrepancies is to calibrate the information estimated using global and open data sets with other available and verifiable sources of data. This can be done, for example, by introducing a factor to correct for the over or underestimation of the indicators at different cluster locations.

However, it is necessary to note that the comparisons shown here reflect only the data sets used for the case study country of Sierra Leone. These discrepancies may exhibit different patterns and magnitudes when applied to other countries. Therefore, it is important to test this method on other case studies, to validate and calibrate the derived input data with locally available and verifiable data, and to exercise judgment on a country-by-country basis.

Furthermore, the above validation exercise was possible only because alternative and locally verified data sets were available. In fact, in the event that such data exists, they may best be used directly as inputs for the analysis. Oftentimes in data-scarce environments, where only global data sets are available, the only way to validate these methods would be to hold consultations with local stakeholders and communities.

There are other aspects of this research that we were unable to validate given time constraints. These include the method for deriving the flood maps, as well as the outputs of the MATCASC model. In terms of the former, we note that a feasible approach is to compare the generated flood maps with historical flood data (e.g., flood maps for historical events as derived from satellite imagery) to assess whether there are comparable patterns of inundation in the country. This is an activity that may be carried out in the near future.

Additionally, notwithstanding the fact that the MATCASC model has previously been validated by its authors (Koc, 2015; Koc et al., 2013), some strategies were considered for validating the outputs of the MATCASC model based on the case study location. A potentially promising approach is proposed by Bialek et al. (2016), who suggest conducting statistical comparisons using data on historical and simulated cascades. This allows one to assess if the simulated cascades have similar statistical characteristics (e.g., distribution of power outage size) to that of real-life events. However, the lack of current access to information on historical cascades proved the execution of this task to be a challenge. Again, this remains an activity that may be carried out in the future, pending data availability.

Finally, the sensitivity analysis results indicate that the assumptions used to assume the spatial distribution of power load and the transmission line property of reactance will meaningfully alter model outcomes. It is thus important for the policy maker to obtain verifiable information that can inform these assumptions to increase the validity of model results.

## 7 Conclusion

This final chapter addresses the research question posed in Chapter 1: “How to overcome data scarcity when analysing the impacts of cascading failures in power networks caused by floods?” The sub-questions are first briefly discussed, after which the proposed method is summarized, answering the main research question. Finally, we discuss the main impacts, limitations, and potential future directions of this research.

### 7.1 Research questions

1. *What are the key components characterizing the research problem that can be derived from global data sets?*

It was found that the following three key components of the research and the necessary information characterizing those components are:

- **Power network:** Network topology, load distribution, substation location coordinates, and network properties (such as substation voltages and transmission line properties)

This research demonstrates a method to derive the power network topology and estimate substation location coordinates using the global data set, GridFinder. The locations and generation capacities of power plants may be obtained from other global data sets such as that provided by AfDB and WRI.

There is no global data set that provides information on substation voltages and transmission line properties in a network. To address this limitation for the case study location, we reviewed and gathered information from published reports on various past projects to support the assumed substation voltages and line properties that were finally modelled. Alternatively, standard type libraries (e.g., from the Pandapower Python package) contain standard line types that can be used based on higher-level information about the power networks in the location of interest.

- **Flood hazard analysis:** Flood maps depicting water heights for multiple return periods, river basin delineations, fragility curves for power network components

The Fathom-Global 2.0 data set provides high-resolution flood maps for multiple return periods, which we used to derive exceedance probability curves for 90m grid cells across the country. The USGS HydroSHEDS database provides a global data set for river basins that can be used in conjunction with the Fathom-Global 2.0 exceedance probability curves to generate flood heights for river basin flood events.

Generalized fragility curves of a power network can be obtained from the HAZUS technical manual, which may then be used to quantify the flood risk of the exposed power network nodes.

- **Impacts assessment:** High-resolution geodemographic data on population characteristics

It was found that the USAID Demographic and Health Surveys program contains representative survey data for over 90 countries. Survey respondents are associated with a cluster, and many of these data sets include GPS coordinates indicating survey cluster locations. Select indicators may be used to calculate cluster-level statistics and, using a geostatistical interpolation method (Empirical Bayesian Kriging), generate maps of that indicator for the country. The metrics that can be used for the impact assessment are limited to the indicators available from the survey.

2. *How does the power network respond to a disruption caused by failed nodes in the network?*

The model results depict how the initial failures propagate through the network and cause a service reduction ranging from 33% to 99%, depending on the initial damage state. Model results also present how the cascade of failures occurs in multiple successive stages.

3. *What are the ways to analyse the impacts of cascading failures in the power network?*

Several metrics were used to evaluate the performance of the network after a cascading failure, including total power lost, size of the population impacted, size of the population from poor households impacted, and size of the population from women-headed households impacted. The metrics provide multiple perspectives for analysing the impacts of the cascading failures and may be selected in accordance with the policy objectives of the decision-maker.

4. *How can the proposed method be used for the analysis of policy interventions?*

The method provides a systematic way to compare the performance of the power network under different interventions. In this study, we demonstrated the implementation of interventions that create redundancies in the network by adding parallel lines along the high-voltage transmission line. Following this, we filtered the best performing policies under each of the metrics discussed previously and evaluated the resulting performance outcomes and trade-offs. Other types of policy interventions may also be considered and tested in the model.

5. *How can the proposed method be adapted to account for uncertain future scenarios?*

The method can be adapted in various ways to account for the impacts of uncertain future scenarios. We demonstrated one way to accomplish this by altering the flood hazard intensities based on a projected change in extreme rainfall in future time periods. For this example, we picked an intermediate climate emissions scenario (RCP4.5). However, more comprehensive analyses may be implemented by taking into account other emissions scenarios and climate indicators. The change in flood risk of the power network in the successive time periods can then be analysed to inform planning decisions.

To answer the main research question, the following method is proposed:

1. Various global data sets are used to derive the national power transmission network and flood maps, and to map population statistics. Context-specific information from various sources may be used to supplement this process.
2. The flood maps and the power network are overlaid to identify network nodes that are exposed to flood risk, and the potential damage states that may occur. The failure rates of the individual nodes are indicative of the levels of the risk at each node.

3. Transmission lines directly connected to the exposed nodes are input into the cascading failures model as initially failed lines, which can be used to simulate the consequent failures that cascade through the network.
4. With the geographic extents of the failures known, local characteristics of the populations affected can be determined and used to measure the impacts of a cascading failure.

Within the case study context, we compared some of the estimated data with verified information to gain an idea of the validity of the proposed method in Sierra Leone. However, it is necessary to apply this method to more case study locations and to conduct more validation exercises, in order to more broadly assess the validity of the proposed method. This remains on the list of future work for this research.

## 7.2 Impact of research

The method proposed in this research allows policy makers working in environments that lack complete or high-resolution data to derive insights on three key findings: (i) which components of the power network are exposed to flood risk, (ii) how failures associated with that flood risk cascade through the rest of the power network, and (iii) the impacts of those cascading failures. These three key findings can be further built upon to analyse other aspects such as potential policy interventions and uncertain future scenarios.

We demonstrate that the method can be flexibly adapted to meet the needs of the policy maker in terms of the following aspects:

1. **Different metrics:** We approached the performance metrics from both utilitarian (size of the power outage / total population affected) and welfare (poor and female-headed households affected) perspectives. However, based on the needs of the audience, the method can be adapted to implement other metrics for impacts quantification (e.g., level of industrial activity in an area as a proxy to estimate potential economic losses).
2. **Different policy levers:** Various other power network improvement methods can be implemented and tested, such as adding new power plants and various other configurations of network expansion.
3. **Different future scenarios:** The method can be used to explore the impacts of a wide range of uncertain scenarios, such as urbanization, migration, or other climate scenarios.
4. **Different climate-related hazards:** Pending the availability of intensity maps and fragility curves for other hazards, this method can be extended to account for other natural disasters.

Given that this study was executed using global data sets, and supplemented by information gathered from miscellaneous data sources (e.g., past project reports), the proposed method opens up the possibility of extending and applying this analysis to countries that are data scarce. The final data inputs used can be supplemented with available data sets for the location of interest to further improve the fidelity of the analysis. However, where high-resolution data is lacking and timely analysis is necessary (thereby precluding the possibility of collecting locally verified data), this method provides policy makers with an avenue to conduct this study with readily available data.

### 7.3 Limitations

This study was limited by several challenges, enumerated as follows:

1. Power network inputs: The GridFinder study is based on approximations and estimations that are further based on open data and other assumptions (as discussed in the article by [Arderne et al. \(2020\)](#)). As this analysis stands heavily on the GridFinder data, we inherit these assumptions accordingly. As shown in the sensitivity analysis (Appendix A.4), the input parameters that vary the outputs of the cascading failures analysis are the reactance properties of the transmission lines and the initial load distribution in the network. Thus, it is important to obtain high confidence data for these inputs.
2. Flood risk analysis
  - This analysis assumed complete independence between flood events across different river basins. This is unlikely to be true, as studies show that there exists a relationship between river basins that can influence relative flood intensities ([Berghuijs, Allen, Harrigan, & Kirchner, 2019](#); [De Luca, Hillier, Wilby, Quinn, & Harrigan, 2017](#)).
  - We linearly interpolated between the 10 (return period) data points to obtain the exceedance probabilities for the flood map cells. However, a study by [Ward, Moel, and Aerts \(2011\)](#) has shown that this approach can underestimate the flood heights (and corresponding damages) for lower return periods/higher frequency floods. One way to address this is to fit a (e.g., beta) distribution to the data points to account for the concavity of the exceedance probability curve between lower return periods.
  - We assumed that pluvial and fluvial floods co-occur with the same intensity. This is unlikely to be true as these flood events, when co-occurring, may concatenate and result in worse outcomes ([A. S. Chen, Djordjević, Leandro, & Savić, 2010](#)).
3. Fragility curves
  - The fragility curves are defined based on parameters found in the HAZUS technical manual. The HAZUS manual was developed by and for United States infrastructures, and use methods and assumptions that may not be applicable to other locations.
  - HAZUS explicitly assumes that electrical equipment is raised to an elevation of 3 ft., which informs the assumed functionality threshold of 4 ft. This obviously may not be the case in other locations. With that said, the sensitivity analysis of the fragility curve parameters indicated that variation in the fragility curve flood heights alters only the specific level of risk associated with each node, and does not alter the risk rankings of the nodes. However, for more accurate quantification of node risks, the fragility curves should be calibrated and validated using inputs from on-the-ground reviewers and locally verified data.
4. Cascading failure model: The MATCASC model used for the cascading failures analysis employs a DC power flow analysis. This involves considering only active power and disregarding the behavior and effects of reactive power in the system. This is relatively inaccurate as compared to AC load flow analyses, and may result in underestimation of power losses (?). However, some studies have shown that the introduced error from using DC power flow analysis can be relatively small ([Van Hertem, Verboomen, Purchala, Belmans, & Kling, 2006](#)).

## 7.4 Future directions of research

Various aspects of the proposed method may be further improved. Firstly, the method should be tested and evaluated using more case studies and compared with locally available data. This is to provide a more comprehensive evaluation of the efficacy of the method. Next, the method for flood risk analysis can be improved by incorporating a deeper understanding of the relationship between river basins, as well as a representation of the co-occurrence of fluvial and pluvial floods, into the method. Additionally, the cascading failures analysis model may be improved by extending the MATCASC model to incorporate AC load flow analysis, and to consider other causes of cascading failures, such as instability of network voltage and frequency. Furthermore, this research sets the ground for a more comprehensive analysis using multi-objective optimization for evaluating and selecting policies, while taking into account deeply uncertain future scenarios.

## References

- African Development Bank, S. (2019). *Mini-grid market opportunity assessment: Sierra leone*. Agency, J. I. C. (2009). *Final report on the master plan study on power supply in western area in the republic of sierra leone*.
- Aidoo, K., & Briggs, R. C. (2019). Underpowered: Rolling blackouts in africa disproportionately hurt the poor. *African Studies Review*, *62*(3), 112–131. doi: <https://doi.org/10.1017/asr.2018.78>
- ArcGIS. (2013). *Empirical bayesian kriging – robust kriging as a geoprocessing tool*. Retrieved from <https://pro.arcgis.com/en/pro-app/latest/help/analysis/geostatistical-analyst/what-is-empirical-bayesian-kriging-.htm>
- Arderne, C., Zorn, C., Nicolas, C., & Koks, E. (2020). Predictive mapping of the global power system using open data. *Scientific data*, *7*(1), 1–12. doi: <https://doi.org/10.1038/s41597-019-0347-4>
- Arif, A., Wang, Z., Wang, J., & Chen, C. (2017). Power distribution system outage management with co-optimization of repairs, reconfiguration, and dg dispatch. *IEEE Transactions on Smart Grid*, *9*(5), 4109–4118. doi: <https://doi.org/10.1109/TSG.2017.2650917>
- Ayyub, B. M. (2014). Systems resilience for multihazard environments: Definition, metrics, and valuation for decision making. *Risk analysis*, *34*(2), 340–355. doi: <https://doi.org/10.1111/risa.12093>
- BBC. (2018). *Sierra leone country profile*. Retrieved from <https://www.bbc.com/news/world-africa-14094194>
- Berghuijs, W. R., Allen, S. T., Harrigan, S., & Kirchner, J. W. (2019). Growing spatial scales of synchronous river flooding in europe. *Geophysical Research Letters*, *46*(3), 1423–1428. doi: <https://doi.org/10.1029/2018GL081883>
- Bialek, J., Ciapessoni, E., Cirio, D., Cotilla-Sanchez, E., Dent, C., Dobson, I., . . . others (2016). Benchmarking and validation of cascading failure analysis tools. *IEEE Transactions on Power Systems*, *31*(6), 4887–4900. doi: <https://doi.org/10.1109/TPWRS.2016.2518660>
- Bienstock, D., & Verma, A. (2010). The nk problem in power grids: New models, formulations, and numerical experiments. *SIAM Journal on Optimization*, *20*(5), 2352–2380. doi: <https://doi.org/10.1137/08073562X>
- Birch, C. P., Oom, S. P., & Beecham, J. A. (2007). Rectangular and hexagonal grids used for observation, experiment and simulation in ecology. *Ecological modelling*, *206*(3-4), 347–359. doi: <https://doi.org/10.1016/j.ecolmodel.2007.03.041>
- Blume, S. W. (2016). *Electric power system basics for the nonelectrical professional*. John Wiley & Sons.
- Blumsack, S. (2006). *Some implications of braess' paradox in electric power systems* (Tech. Rep.). Citeseer.
- Bouwer, L. M. (2011). Have disaster losses increased due to anthropogenic climate change? *Bulletin of the American Meteorological Society*, *92*(1), 39–46. doi: <https://doi.org/10.1175/2010BAMS3092.1>
- Brown, T., Hörsch, J., & Schlachtberger, D. (2018). PyPSA: Python for Power System Analysis. *Journal of Open Research Software*, *6*(4). Retrieved from <https://doi.org/10.5334/jors.188> doi: <https://doi.org/10.5334/jors.188>
- Buldyrev, S. V., Parshani, R., Paul, G., Stanley, H. E., & Havlin, S. (2010). Catastrophic cascade of failures in interdependent networks. *Nature*, *464*(7291), 1025–1028. doi: <https://doi.org/10.1038/nature08932>
- Burlando, A. (2011). The impact of electricity on work and health: evidence from a blackout in zanzibar. *SSRN Electronic Journal*. doi: <https://doi.org/10.2139/ssrn.1734525>

- Bustos-Turu, G., van Dam, K. H., Acha, S., Markides, C. N., & Shah, N. (2016). Simulating residential electricity and heat demand in urban areas using an agent-based modelling approach. In *2016 IEEE International Energy Conference (EnergyCon)* (pp. 1–6). doi: <https://doi.org/10.1109/ENERGYCON.2016.7514077>
- Chen, A. S., Djordjević, S., Leandro, J., & Savić, D. (2010). An analysis of the combined consequences of pluvial and fluvial flooding. *Water Science and Technology*, *62*(7), 1491–1498. doi: <https://doi.org/10.2166/wst.2010.486>
- Chen, C., Wang, J., Qiu, F., & Zhao, D. (2015). Resilient distribution system by microgrids formation after natural disasters. *IEEE Transactions on Smart Grid*, *7*(2), 958–966. doi: <https://doi.org/10.1109/TSG.2015.2429653>
- Chen, S., Compare, M., & Zio, E. (2019). Agent-based modeling for energy supply chain resilience analysis. Research Publishing. doi: <https://doi.org/10.3850/978-981-11-2724-3>
- Cicilio, P., Swartz, L., Vaagensmith, B., Rieger, C., Gentle, J., McJunkin, T., & Cotilla-Sanchez, E. (2020). Electrical grid resilience framework with uncertainty. *Electric Power Systems Research*, *189*, 106801. doi: <https://doi.org/10.1016/j.epsr.2020.106801>
- Clark-Ginsberg, A. (2016). What’s the difference between reliability and resilience? *Department of Homeland Security*. doi: <https://doi.org/10.13140/RG.2.2.20571.46885>
- Climate Change Knowledge Portal. (n.d.). Retrieved from <http://climateknowledgeportal.worldbank.org>
- Cuadra, L., Salcedo-Sanz, S., Del Ser, J., Jiménez-Fernández, S., & Geem, Z. W. (2015). A critical review of robustness in power grids using complex networks concepts. *Energies*, *8*(9), 9211–9265. doi: <https://doi.org/10.3390/en8099211>
- De Luca, P., Hillier, J. K., Wilby, R. L., Quinn, N. W., & Harrigan, S. (2017). Extreme multi-basin flooding linked with extra-tropical cyclones. *Environmental Research Letters*, *12*(11), 114009. doi: <https://doi.org/10.1088/1748-9326/aa868e>
- Doll, C. N., & Pachauri, S. (2010). Estimating rural populations without access to electricity in developing countries through night-time light satellite imagery. *Energy Policy*, *38*(10), 5661–5670. doi: <https://doi.org/10.1016/j.enpol.2010.05.014>
- Electricity Distribution and Supply Authority. (2019). *Environmental social and health impact assessment: Final report 2019*. Retrieved from [https://ewsdata.rightsindevelopment.org/files/documents/90/WB-P166390\\_8ak94QK.pdf](https://ewsdata.rightsindevelopment.org/files/documents/90/WB-P166390_8ak94QK.pdf)
- Energy Sector Management Assistance Program. (2019). *Mini grids for half a billion people: Market outlook and handbook for decision makers*. World Bank.
- European Commission. (2004). Communication from the commission to the council and the european parliament-critical infrastructure protection in the fight against terrorism, com/2004/0702-final.
- Federal Emergency Management Agency. (n.d.). Hazus-mh flood model technical manual [Computer software manual]. (Accessed: 2021-03-28)
- for Economic Co-operation, O., & Development. (2017). *Development co-operation report 2017*. Retrieved from <https://www.oecd-ilibrary.org/content/publication/dcr-2017-en> doi: <https://doi.org/10.1787/dcr-2017-en>
- Guo, H., Zheng, C., Iu, H. H.-C., & Fernando, T. (2017). A critical review of cascading failure analysis and modeling of power system. *Renewable and Sustainable Energy Reviews*, *80*, 9–22. doi: <https://doi.org/10.1016/j.rser.2017.05.206>
- Hagberg, A. A., Schult, D. A., & Swart, P. J. (2008). Exploring network structure, dynamics, and function using networkx. In G. Varoquaux, T. Vaught, & J. Millman (Eds.), *Proceedings of the 7th python in science conference* (p. 11 - 15). Pasadena, CA USA.
- He, X. (2018). Disaster risk assessment for community resilience: A case study for Jamaica.
- Helton, J. C., & Davis, F. J. (2003). Latin hypercube sampling and the propagation of uncer-

- tainty in analyses of complex systems. *Reliability Engineering & System Safety*, 81(1), 23–69. doi: [https://doi.org/10.1016/S0951-8320\(03\)00058-9](https://doi.org/10.1016/S0951-8320(03)00058-9)
- International Development Association. (2020). *Project appraisal document on a proposed grant for enhancing sierra leone energy access*.
- International Labour Organization. (2008). *Infrastructure, poverty reduction and jobs*. Retrieved from [https://www.ilo.org/global/docs/WCMS\\_099513/lang--en/index.htm](https://www.ilo.org/global/docs/WCMS_099513/lang--en/index.htm)
- Jeong, S.-H., & Elnashai, A. S. (2007). Probabilistic fragility analysis parameterized by fundamental response quantities. *Engineering Structures*, 29(6), 1238–1251. doi: <https://doi.org/10.1016/j.engstruct.2006.06.026>
- Jufri, F. H., Kim, J.-S., & Jung, J. (2017). Analysis of determinants of the impact and the grid capability to evaluate and improve grid resilience from extreme weather event. *Energies*, 10(11), 1779. doi: <https://doi.org/10.3390/en10111779>
- Kennedy, R. P., Cornell, C. A., Campbell, R., Kaplan, S., & Perla, H. (1980). Probabilistic seismic safety study of an existing nuclear power plant. *Nuclear Engineering and Design*, 59(2), 315–338. doi: [https://doi.org/10.1016/0029-5493\(80\)90203-4](https://doi.org/10.1016/0029-5493(80)90203-4)
- Kesselring, R. (2017). The electricity crisis in zambia: Blackouts and social stratification in new mining towns. *Energy Research & Social Science*, 30, 94–102. doi: <https://doi.org/10.1016/j.erss.2017.06.015>
- Koc, Y. (2015). *Measuring the robustness of power grids: A complex networks theory approach* (Unpublished doctoral dissertation). Delft University of Technology.
- Koc, Y., Verma, T., Araujo, N. A., & Warnier, M. (2013). Matcasc: A tool to analyse cascading line outages in power grids. In *2013 ieee international workshop on intelligent energy systems (iwies)* (pp. 143–148). doi: <https://doi.org/10.1109/IWIES.2013.6698576>
- Kojima, M., & Trimble, C. (2016). Making power affordable for africa and viable for its utilities.
- Krivoruchko, K., & Gribov, A. (2019). Evaluation of empirical bayesian kriging. *Spatial Statistics*, 32, 100368. doi: <https://doi.org/10.1016/j.spasta.2019.100368>
- Lehner, B., Verdin, K., & Jarvis, A. (2008). New global hydrography derived from spaceborne elevation data. *Eos, Transactions American Geophysical Union*, 89(10), 93–94. doi: <https://doi.org/10.1029/2008EO100001>
- Lempert, R. J. (2003). *Shaping the next one hundred years: new methods for quantitative, long-term policy analysis*. Rand Corporation.
- Lloyd, C. T., Sorichetta, A., & Tatem, A. J. (2017). High resolution global gridded data for use in population studies. *Scientific data*, 4(1), 1–17. doi: <https://doi.org/10.1038/sdata.2017.1>
- Masereka, E. M., Ochieng, G. M., & Snyman, J. (2018). Statistical analysis of annual maximum daily rainfall for nelspruit and its environs. *Jàmbá: Journal of Disaster Risk Studies*, 10(1), 1–10. doi: <https://dx.doi.org/10.4102/jamba.v10i1.499>
- Ministry of Energy, Government of Sierra Leone. (2019). *Electricity sector reform roadmap (2017-2030)*. Retrieved from <https://rise.esmap.org/data/files/library/sierra-leone/Energy%20Access/EA%2014.1B.pdf>
- Ministry of Energy Sierra Leone. (2017). *Progress report (2014-2017)*. Retrieved from <http://www.energy.gov.sl/wp-content/uploads/2018/04/ProgressReportMoE.pdf>
- Najibi, N., & Devineni, N. (2018). Recent trends in the frequency and duration of global floods. *Earth System Dynamics*, 9(2), 757–783. doi: <https://doi.org/10.5194/esd-9-757-2018>
- National Water Resources Management Agency Sierra Leone. (2015). *Map 1: Sierra leone's river basins*. Retrieved from <https://www.salonewatersecurity.com/maps>
- Nicholls, R. J., Hoozemans, F. M., & Marchand, M. (1999). Increasing flood risk and wetland losses due to global sea-level rise: regional and global analyses. *Global Environmental Change*, 9, S69–S87. doi: [https://doi.org/10.1016/S0959-3780\(99\)00019-9](https://doi.org/10.1016/S0959-3780(99)00019-9)
- North American Electric Reliability Corporation. (2013). *Reliability terminology*. Author.

- Sampson, C. C., Smith, A. M., Bates, P. D., Neal, J. C., Alfieri, L., & Freer, J. E. (2015). A high-resolution global flood hazard model. *Water resources research*, 51(9), 7358–7381. doi: <https://doi.org/10.1002/2015WR016954>
- Sánchez-Muñoz, D., Domínguez-García, J. L., Martínez-Gomariz, E., Russo, B., Stevens, J., & Pardo, M. (2020). Electrical arid risk assessment against flooding in barcelona and bristol cities. *Sustainability*, 12(4), 1527. doi: <https://doi.org/10.3390/su12041527>
- Sen, A. (1979). Utilitarianism and welfarism. *The journal of Philosophy*, 76(9), 463–489. doi: <https://doi.org/10.2307/2025934>
- Sheng, Y., Carrillo-Rodriguez, J., Eun-Young, L., Perez-Ludena, M., & Mukherjee, A. (2007). Access to basic services for the poor: the importance of good governance. Retrieved from <http://digitallibrary.un.org/record/605509> (Published by the UN-ESCAP/UNDP/ADB project on MDGs of Asia and the Pacific.)
- Sierra leone hazard profile*. (n.d.). Retrieved from <http://www.harpis-sl.website/index.php/hazard-profiles/sierra-leone-hazard-profile>
- Statistics Sierra Leone and ICF. (2020). *Sierra leone demographic and health survey 2019*. ([Dataset])
- Sun, K., Han, Z.-X., Cao, Y.-J., et al. (2005). Review on models of cascading failure in complex power grid [j]. *Power System Technology*, 13, 1–9. Retrieved from [https://en.cnki.com.cn/Article\\_en/CJFDTotat-DWJS200513000.htm](https://en.cnki.com.cn/Article_en/CJFDTotat-DWJS200513000.htm)
- The African Development Bank Group. (2021). *Sierra leone - rehabilitation and extension of bo-kenema distribution system project*. The African Development Bank Group. Retrieved from <https://projectsportal.afdb.org/dataportal/VProject/show/P-SL-F00-007>
- The World Bank Group. (2017). *Enterprise surveys*. Retrieved from <www.enterprisesurveys.org>
- The World Bank Group. (2019). *Sierra leone overview*. The World Bank Group. Retrieved from <https://www.worldbank.org/en/country/sierraleone/overview>
- The World Bank Group. (2020). *Report no. 148025-sl country partnership framework for republic of sierra leone for the period fy21-fy26*. The World Bank Group.
- Thurner, L., Scheidler, A., Schafer, F., Menke, J. H., Dollichon, J., Meier, F., ... Braun, M. (2018). pandapower - an open source python tool for convenient modeling, analysis and optimization of electric power systems. *IEEE Transactions on Power Systems*. Retrieved from <https://arxiv.org/abs/1709.06743> doi: 10.1109/TPWRS.2018.2829021
- Toole, G. L., & McCown, A. W. (2008). Interdependent energy infrastructure simulation system. *Wiley Handbook of Science and Technology for Homeland Security*, 1–1. doi: <https://doi.org/10.1002/9780470087923.hhs240>
- United Nations. (2015). Transforming our world : the 2030 agenda for sustainable development. Retrieved from <https://sustainabledevelopment.un.org/post2015/transformingourworld/publication>
- United Nations, Department of Economic and Social Affairs, Population Division. (2018). World urbanization prospects: The 2018 revision, online edition.
- United Nations Economic and Social Commission for Asia and the Pacific (UN ESCAP). (2019). *Asia-pacific disaster report 2019 - the disaster riskscape across asia-pacific*. Retrieved from <https://www.unescap.org/publications/asia-pacific-disaster-report-2019#>
- United Nations Economic and Social Commission for Asia and the Pacific (UN ESCAP). (2020). *Ready for the dry years: Building resilience to drought in south-east asia (2nd edition)*. Retrieved from <https://www.unescap.org/publications/ready-dry-years-building-resilience-drought-south-east-asia-2nd-edition#>
- United Nations Economic and Social Commission for Asia and the Pacific (UN ESCAP). (2021)

- forthcoming). *Asia-pacific disaster report 2021*.
- United Nations Office for Disaster Risk Reduction. (2020). Annual report 2020.
- Vaiman, M., Bell, K., Chen, Y., Chowdhury, B., Dobson, I., Hines, P., ... Zhang, P. (2012). Risk assessment of cascading outages: Methodologies and challenges. *IEEE Transactions on Power Systems*, *27*(2), 631. doi: <https://doi.org/10.1109/TPWRS.2011.2177868>
- Van Hertem, D., Verboomen, J., Purchala, K., Belmans, R., & Kling, W. L. (2006). Usefulness of dc power flow for active power flow analysis with flow controlling devices. doi: <https://doi.org/10.1049/cp:20060013>
- Verwey, A., Kerblat, Y., & Chia, B. (2017). *Flood risk management at river basin scale: The need to adopt a proactive approach*. World Bank.
- Wang, J., Zuo, W., Rhode-Barbarigos, L., Lu, X., Wang, J., & Lin, Y. (2019). Literature review on modeling and simulation of energy infrastructures from a resilience perspective. *Reliability Engineering & System Safety*, *183*, 360–373. doi: <https://doi.org/10.1016/j.res.2018.11.029>
- Ward, P. J., Moel, H. d., & Aerts, J. (2011). How are flood risk estimates affected by the choice of return-periods? *Natural Hazards and Earth System Sciences*, *11*(12), 3181–3195. doi: <https://doi.org/10.5194/nhess-11-3181-2011>
- Witthaut, D., & Timme, M. (2012). Braess's paradox in oscillator networks, desynchronization and power outage. *New journal of physics*, *14*(8), 083036. doi: <https://doi.org/10.1088/1367-2630/14/8/083036>
- Zhang, P., & Peeta, S. (2011). A generalized modeling framework to analyze interdependencies among infrastructure systems. *Transportation Research Part B: Methodological*, *45*(3), 553–579. doi: <https://doi.org/10.1016/j.trb.2010.10.001>
- Zimmerman, R. D., Murillo-Sánchez, C. E., & Thomas, R. J. (2010). Matpower: Steady-state operations, planning, and analysis tools for power systems research and education. *IEEE Transactions on power systems*, *26*(1), 12–19. doi: <https://doi.org/10.1109/TPWRS.2010.2051168>
- Zorn, C., Pant, R., Thacker, S., & Shamseldin, A. Y. (2020). Evaluating the magnitude and spatial extent of disruptions across interdependent national infrastructure networks. *ASCE-ASME J Risk and Uncert in Engrg Sys Part B Mech Engrg*, *6*(2). doi: <https://doi.org/10.1115/1.4046327>

## A Appendix

The appendix includes the following:

- [A.1](#): A list and depiction of all the policy options explored in this study.
- [A.2](#): Maps depicting the cascade of failures for each damage state scenario.
- [A.3](#): Results from validation exercise.
- [A.4](#): Results from sensitivity analysis.

## A.1 Policy Options

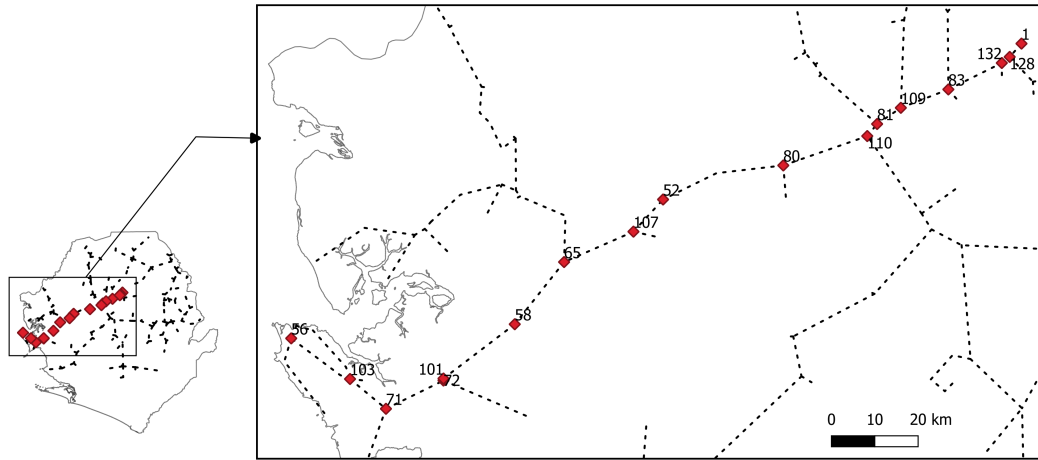


Figure 35: IDs of nodes on high-voltage line from Bumbuna to Freetown in Sierra Leone.

Policy	Start node	End node	Policy	Start node	End node	Policy	Start node	End node	Policy	Start node	End node
Policy0	1	52	Policy30	56	71	Policy60	65	110	Policy90	81	101
Policy1	1	56	Policy31	56	72	Policy61	65	128	Policy91	81	103
Policy2	1	58	Policy32	56	80	Policy62	65	132	Policy92	81	107
Policy3	1	65	Policy33	56	81	Policy63	71	80	Policy93	81	128
Policy4	1	71	Policy34	56	83	Policy64	71	81	Policy94	81	132
Policy5	1	72	Policy35	56	101	Policy65	71	83	Policy95	83	101
Policy6	1	80	Policy36	56	107	Policy66	71	101	Policy96	83	103
Policy7	1	81	Policy37	56	109	Policy67	71	107	Policy97	83	107
Policy8	1	83	Policy38	56	110	Policy68	71	109	Policy98	83	110
Policy9	1	101	Policy39	56	128	Policy69	71	110	Policy99	83	128
Policy10	1	103	Policy40	56	132	Policy70	71	128	Policy100	101	103
Policy11	1	107	Policy41	58	71	Policy71	71	132	Policy101	101	107
Policy12	1	109	Policy42	58	72	Policy72	72	80	Policy102	101	109
Policy13	1	110	Policy43	58	80	Policy73	72	81	Policy103	101	110
Policy14	1	132	Policy44	58	81	Policy74	72	83	Policy104	101	128
Policy15	52	56	Policy45	58	83	Policy75	72	103	Policy105	101	132
Policy16	52	58	Policy46	58	103	Policy76	72	107	Policy106	103	107
Policy17	52	65	Policy47	58	107	Policy77	72	109	Policy107	103	109
Policy18	52	71	Policy48	58	109	Policy78	72	110	Policy108	103	110
Policy19	52	72	Policy49	58	110	Policy79	72	128	Policy109	103	128
Policy20	52	81	Policy50	58	128	Policy80	72	132	Policy110	103	132
Policy21	52	83	Policy51	58	132	Policy81	80	81	Policy111	107	109
Policy22	52	101	Policy52	65	71	Policy82	80	83	Policy112	107	110
Policy23	52	103	Policy53	65	72	Policy83	80	101	Policy113	107	128
Policy24	52	109	Policy54	65	80	Policy84	80	103	Policy114	107	132
Policy25	52	110	Policy55	65	81	Policy85	80	107	Policy115	109	110
Policy26	52	128	Policy56	65	83	Policy86	80	109	Policy116	109	128
Policy27	52	132	Policy57	65	101	Policy87	80	128	Policy117	109	132
Policy28	56	58	Policy58	65	103	Policy88	80	132	Policy118	110	128
Policy29	56	65	Policy59	65	109	Policy89	81	83	Policy119	110	132

Table 3: Enumeration of all policies considered in the analysis.

## A.2 Cascading failures in each damage state scenario

The following shows the maps representing the cascading failures in each damage state scenario. The load clusters that experience the initial outage is colored in light pink, while the clusters that experience an outage in later stages of the cascade are colored in darker shades of red. Areas that do not suffer a power outage are shown in green.

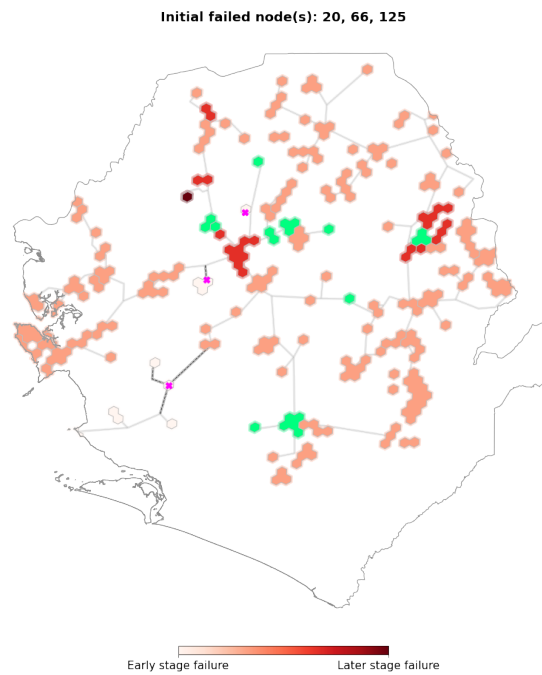


Figure 36: Visual representation of the cascading failure that occurs with the failure of individual nodes 20, 66 and 125.

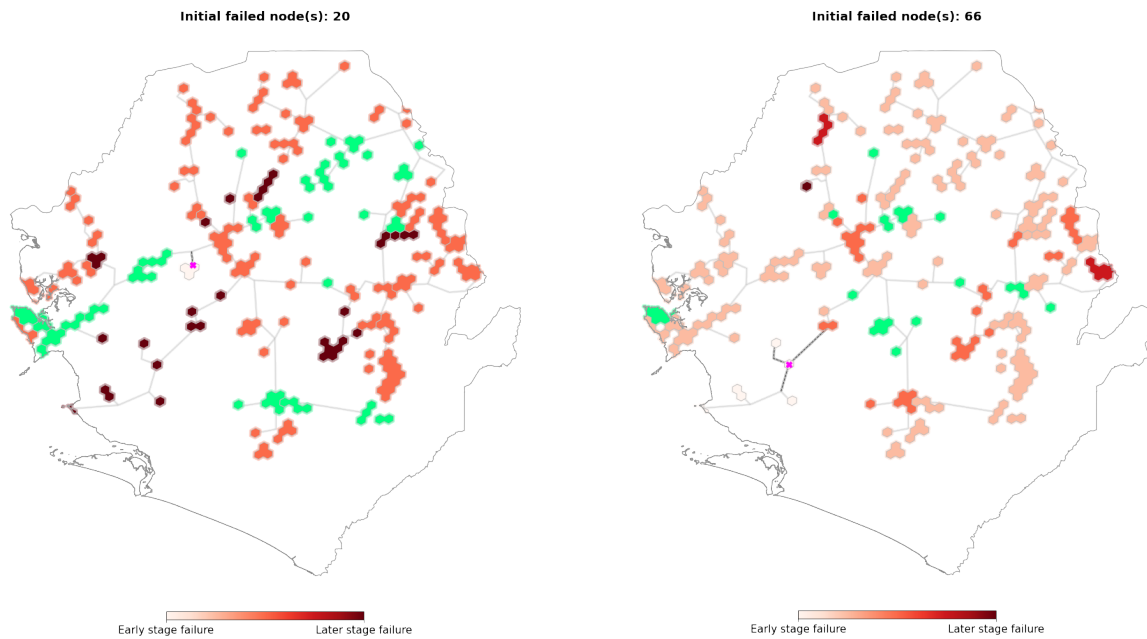


Figure 37: Visual representation of the cascading failure that occurs with the failure of individual node 20 (left) and node 66 (right).

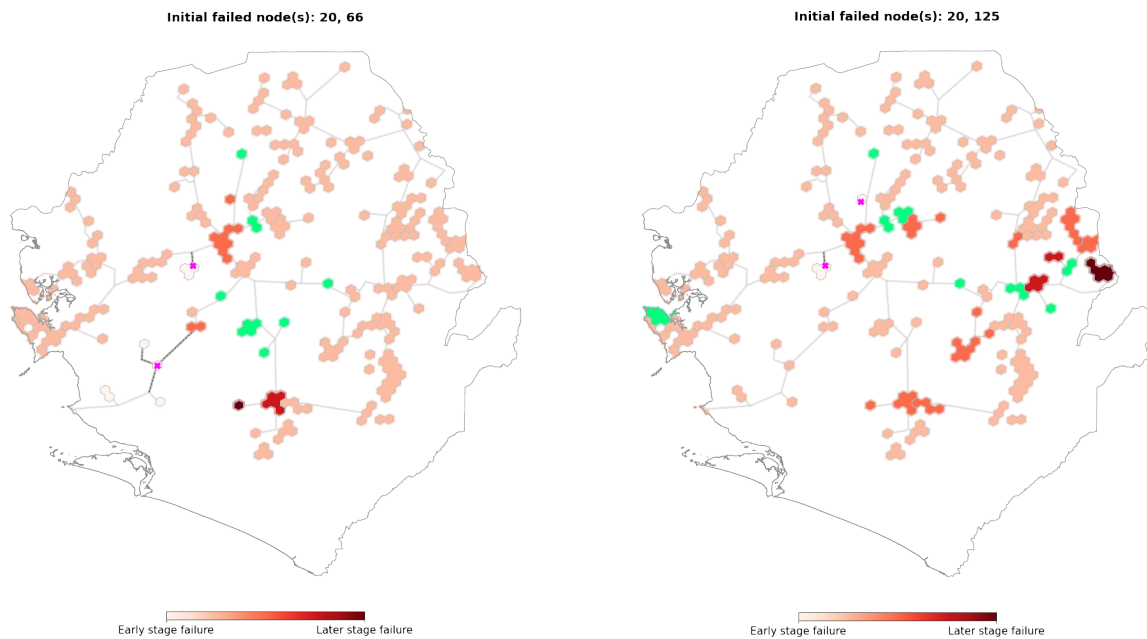


Figure 38: Visual representation of the cascading failure that occurs with the failure of individual nodes 20/66 (left) and nodes 20/125 (right).

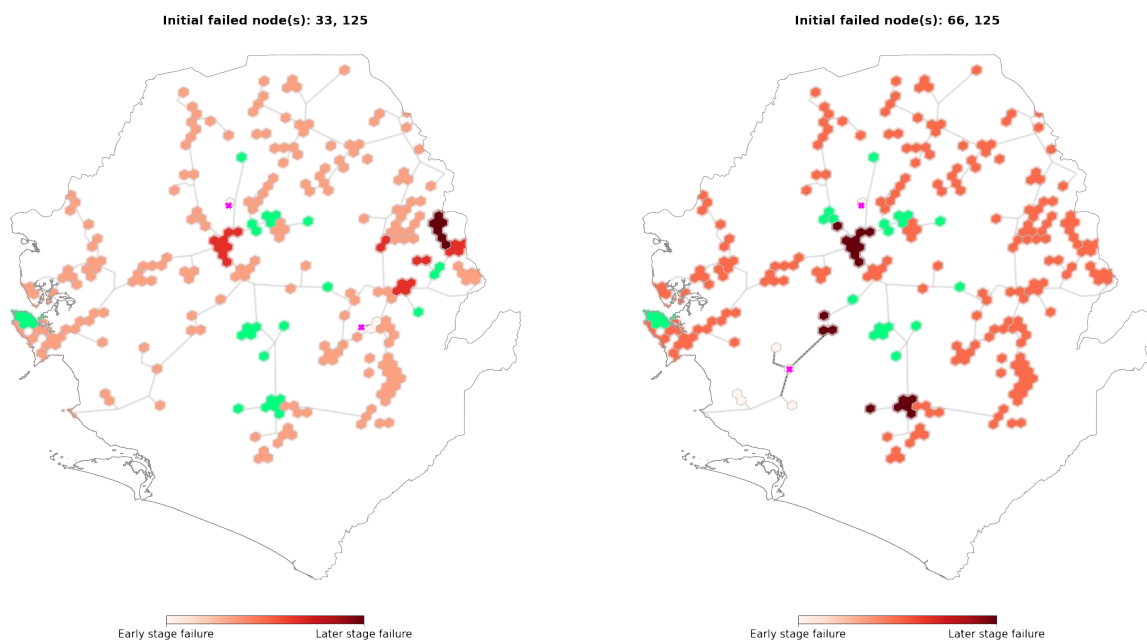


Figure 39: Visual representation of the cascading failure that occurs with the failure of individual nodes 33/125 (left) and nodes 66/125 (right).

### A.3 Validation

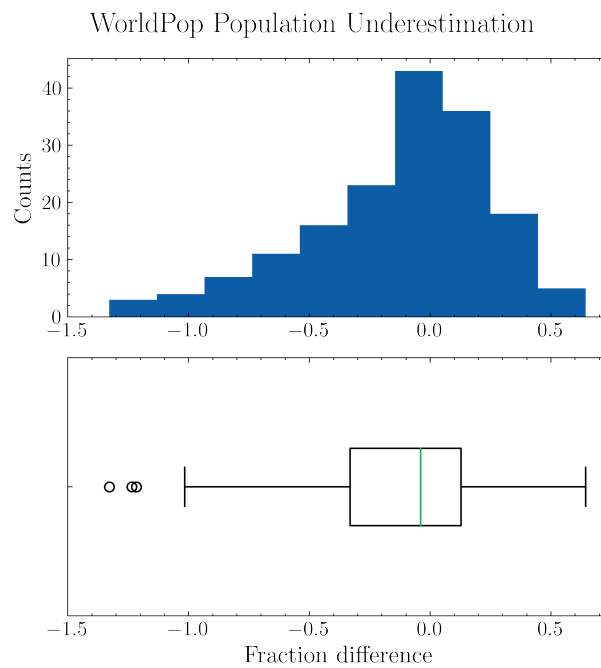


Figure 40: Distribution of discrepancies between WorldPop and census estimates. Positive values indicate underestimation, negative values indicate overestimation.

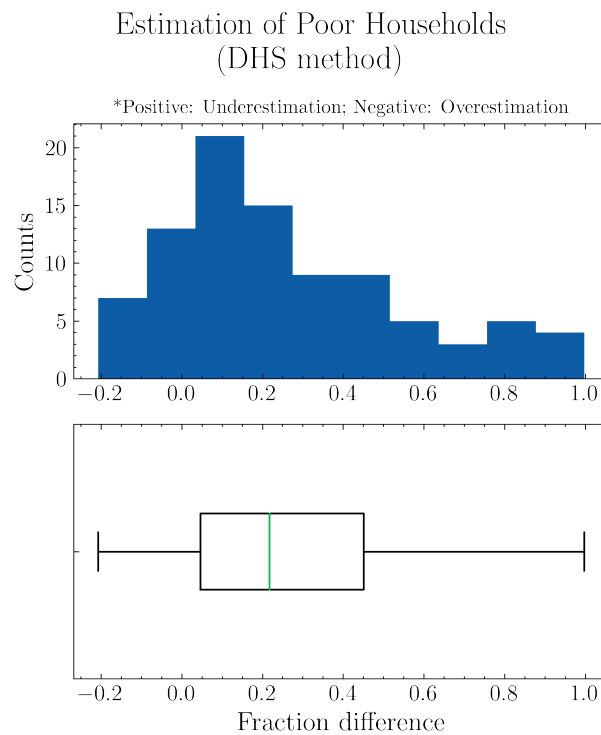


Figure 41: Distribution of discrepancies between DHS survey interpolation estimates and census estimates for poor households.

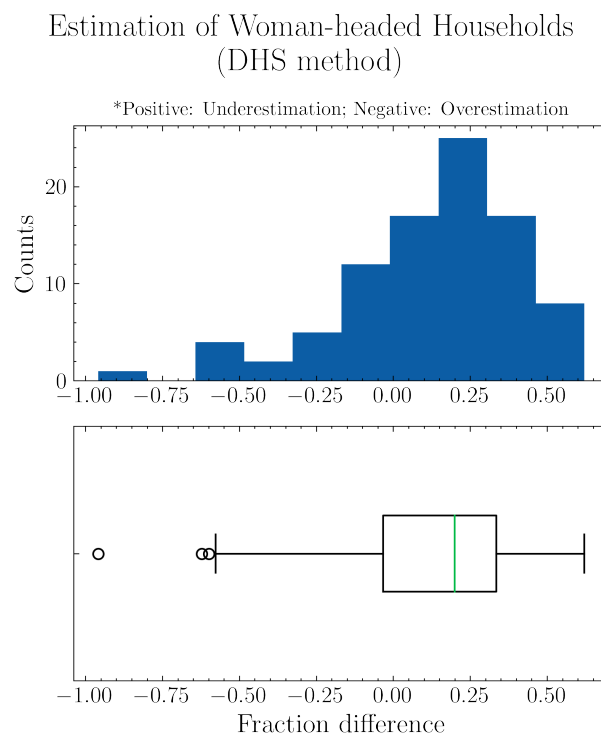


Figure 42: Distribution of discrepancies between DHS survey interpolation estimates and census estimates for women-headed households.

### A.4 Sensitivity Analysis

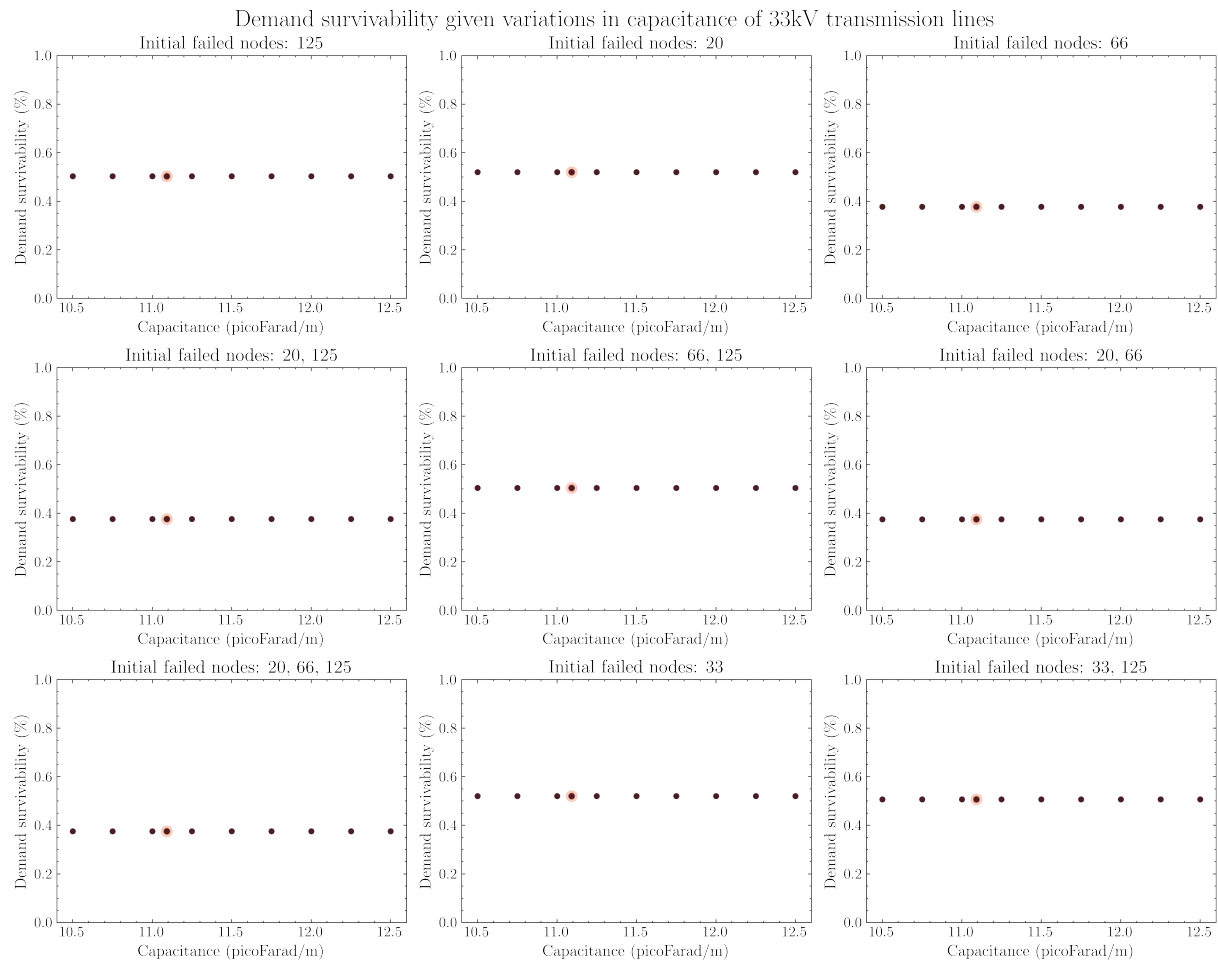


Figure 43: Scatter plots showing change in network performance given variations in transmission line capacitance in each damage state scenario.

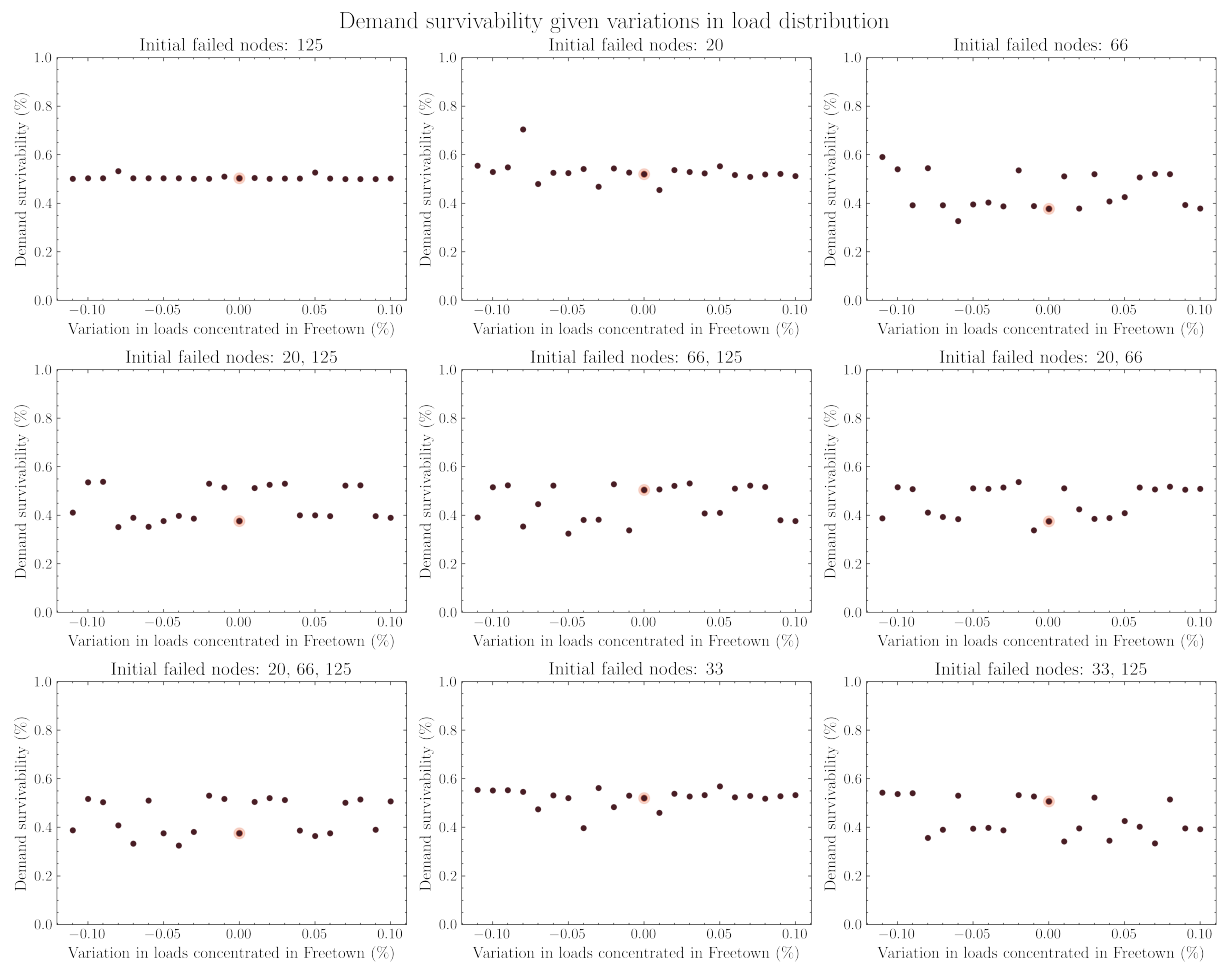


Figure 44: Scatter plots showing change in network performance given variations in spatial distribution of loads in each damage state scenario.

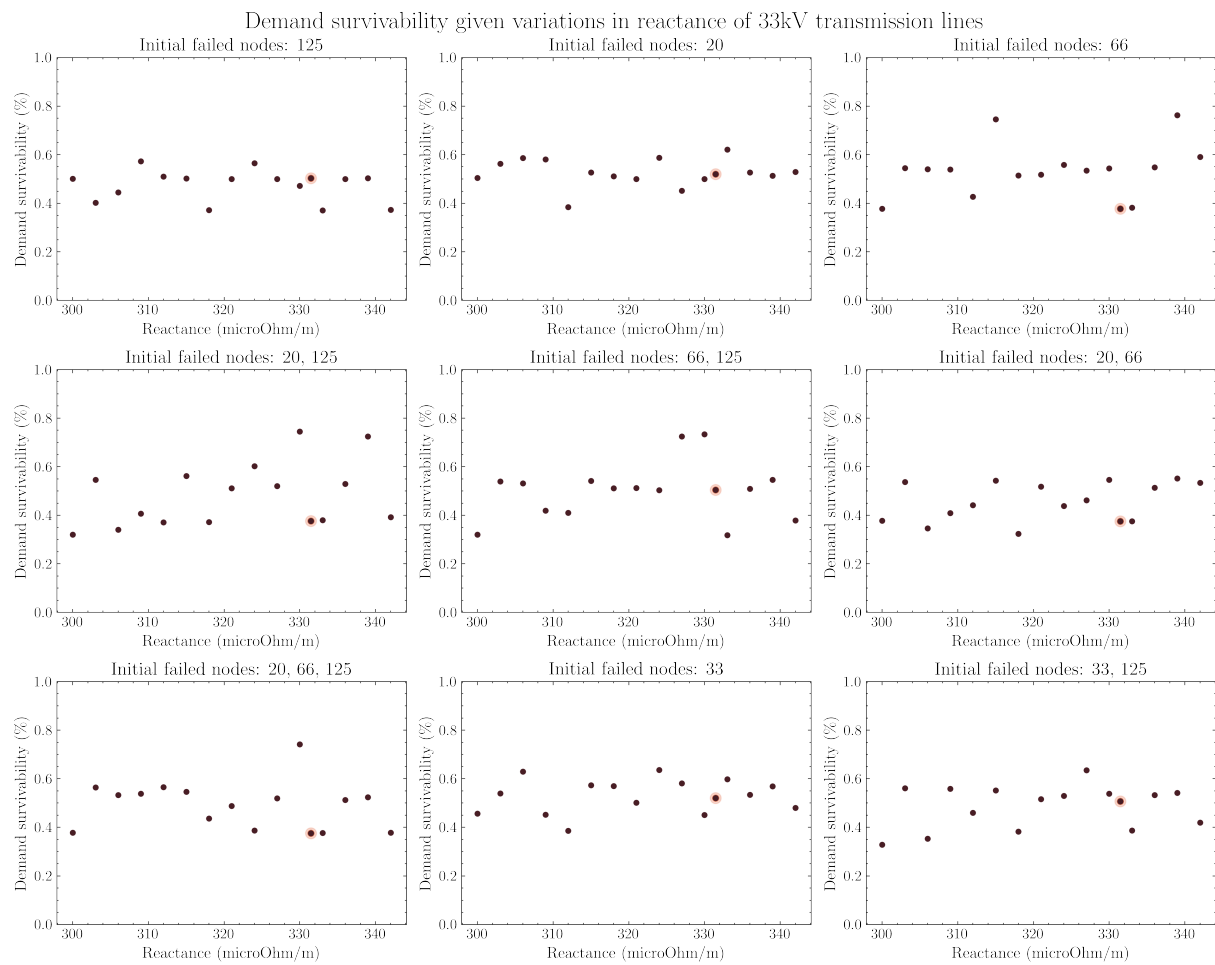


Figure 45: Scatter plots showing change in network performance given variations in transmission line reactance in each damage state scenario.